# WIND TUNNEL TESTS EMPLOYING TEMPORAL AND SPATIAL VARIATIONS IN MASS TRANSFER DISTRIBUTION THROUGH A CONICAL SURFACE TO CONTROL AERODYNAMIC PITCHING MOMENT CHARACTERISTICS

FLUIDYNE ENGINEERING CORP.

# FOREWORD

The work described in this report was carried out as a part of a program to investigate the effects of mass transfer on the stability of re-entry type vehicles. In addition to the work reported here, theoretical investigations were made of the aerodynamic processes involved and these are described in a companion report. The overall program was supported by the Advanced Research Projects Agency, Ballistic Missile Defense Office, Penetration Aids Branch, and was technically administered by the Fluid Dynamics Branch of the Office of Naval Research. The development of an apparatus as complex and sophisticated as that employed in these studies requires the expert skills and devotion of many people. The authors wish to acknowledge the contribution of their co-workers in general and in particular, Messrs. DeCoursin and Lindahl for contributions to the development of the concepts of test apparatus, and Messrs. Estel and Matsuura for their contributions to the solution of the many detailed problems which arose in converting these concepts into a working apparatus.

## ABSTRACT

This report describes an experimental study of the effects of mass transfer on the stability of conical bodies. A unique apparatus was created which permits the support of a conical model in a hypersonic wind tunnel with small pitch damping due to the apparatus, and at the same time provides a means for blowing through four separate (aft, forward, top, bottom combinations) model surface areas. Independent servo controls were provided for the flow through each surface section such that the mass transfer through the model wall could be varied both spatially and temporally. This apparatus was installed in the FluiDyne Hypersonic Wind Tunnel and tests were run at a nominal Mach number of 11. Runs were made without mass transfer, with mass transfer produced by a subliming material, and with mass transfer produced by blowing through a porous surface. These tests provided additional confirmation that mass transfer from a surface will, in itself, significantly influence the pitch damping characteristics of a conical shape, whether its origin is in a heat transfer related phenomenon (such as ablation or sublimation) or an independently controlled flow process such as is represented by blowing through the conical surface. In addition, these tests provided an opportunity for shakedown of the blowing flow control apparatus; however, it was not possible to carry the blowing study into the parametric investigation initially planned within the present program. Thus, the interrelation of such parameters as mass flow, volume flow, spatial distribution, temporal distribution, etc., remain to be investigated in detail.

TABLE OF CONTENTS

# LIST OF TABLES

# LIST OF FIGURES

## NOTATION

| | |
|---|---|
| CG | Center of gravity |
| $C_{M_\alpha}$ | Static stability derivative |
| $C_{M_q}+C_{M_{\dot\alpha}}$ | Dynamic stability derivative |
| d | Model base diameter |
| f | Model oscillation frequency, cps |
| I | Moment of inertia |
| L | Model length |
| m | Mass |
| M | Mach number |
| $M_{\dot\theta}$ | Damping moment parameter |
| P | Pressure or perfect gas |
| q | Dynamic pressure |
| r | Radius |
| R | Gas constant, 1716 $ft^2/sec^2 °R$ |
| Re | Reynolds number |
| S | Model base area |
| $S_{Ab}$ | Ablation area |
| T | Temperature, °R |
| TP | Thermally perfect gas |
| t | Time |
| V | Test section flow velocity |
| x | Axial distance from the vehicle apex |
| ρ | Mass per unit volume, density |
| θ | Amplitude of oscillation |
| ω | Angular oscillation frequency, (2πf) rad/sec |
| λ | Phase shift |
| o | Free stream total |
| ∞ | Free stream static |
| b | Base |
| n | Nose |

# 1.0 INTRODUCTION

This report describes the experimental apparatus which was developed to study the influence of mass transfer from a surface on the dynamic stability of a conical vehicle during hypersonic flight, and the results of a series of wind tunnel tests employing this apparatus.

Exploratory wind tunnel tests which were conducted at FluiDyne Engineering Corporation in 1963 demonstrated that mass transfer from the surface of a conical re-entry body can have a significant effect on the pitch damping coefficients of such a body (Reference 1). The magnitude of this effect was found to be sufficient to reverse the natural stability characteristics of the body, provided the distribution of the mass transfer was of the necessary form. Very generally, mass transfer from areas forward of the center of oscillation appeared to stabilize a body whereas mass transfer from areas aft of the center of oscillation tend to destabilize it. The importance of these effects as regards vehicle design and the prediction of performance characteristics was immediately apparent. Thus the existence of a significant aerodynamic phenomenon had been demonstrated; the immediate problem then became one of analyzing this phenomenon in sufficient detail, by both theoretical and experimental means, to identify the governing parameters involved and develop the equations relating these parameters to the observed results.

In the case of actual flight vehicles the basic mechanism by which mass is transferred from the vehicle

surface is the ablation of material placed on the surface to protect the interior from overheating. From both a theoretical and experimental point of view, the inclusion of parameters which define the ablation process itself into the study of the effects of the product thereof on vehicle aerodynamics leads to an extremely complex problem. Hence, while it was recognized that the ablation process and the aerodynamic flow process are interrelated, it seemed desirable to attack the experimental study of the aerodynamic process as a mass transfer problem without attempting true simulation of the ablation process. Although the aerodynamic process itself is very complex (the effects of temporal and spatial variations in mass addition and the effects of the properties of the fluid being added must be expected to be significant and specifically accounted for) it should be possible to develop a basis for predicting the effect on the overall flow process, and thus the vehicle dynamics, of a given mass addition flow. With this in hand the characteristics of the ablation process which interact significantly with the flow process as regards vehicle stability can be identified, and the effect of a given ablation process predicted.

The current program evolved from these general considerations, with early experimental work being performed on a side supported model for which the bearing was located outside of the wind tunnel flow. While the geometrical arrangement in this early apparatus limited the degree of simulation which could be achieved, tests were run with blowing through a porous surface of the model to simulate ablation and the results obtained (Reference 2) conclusively established that the basic phenomenon previously observed as a characteristic of ablating vehicles could be produced by a relatively simple mass addition flow.

Concurrent with this early experimental work theoretical studies were carried out (and reported in Reference 3) which also confirmed that the observed effects could be produced by a simple mass addition flow. Both of these early results, while generally significant in establishing that a complex interaction between an ablation process and the flow process is not a requirement for producing an effect on vehicle stability, left the development and confirmation of a means of predicting performance in any given case to be achieved.

In order to provide confirmation of a theoretically developed technique for predicting performance and/or to provide the empirical results and coefficients often necessary to establish a base from which a basically sound theory can be used to predict quantitative results, it is necessary to carry out an orderly set of experiments in which the various major parameters can be varied independently over an adequate range. In the present case this requirement led to the design and fabrication of a test apparatus specifically for the purpose of studying the effects of varying the principal mass flow parameters on the stability of a conical vehicle. This apparatus, which is described in detail in the following report, consists of a conical model supported byan internal air bearing which in turn is supported from a conventional aft sting. The model is compartmented so that blowing forward, aft, windward, and leeward can be independently varied, and the flow through each compartment is controlled by a servo system such that the flow can be varied with time in terms of the form of flow versus time curve and the displacement of this curve with respect to the model motion. Provision was made in the development of this system to permit

its use in testing with subliming materials, such as paradichlorobenzene and ammonium chloride, and with blowing gases other than air. Because of the complexity of the system, a great deal of difficulty was encountered in placing it in operational status; thus the air bearing with its integral blowing channels, the frictionless angle of attack transducer, the miniaturized flow control valves and their electrohydraulic servo control systems, all represented the development of new operational systems involving sophisticated engineering concepts. The development of this equipment culminated in its use in carrying out additional wind tunnel studies of the effect of mass transfer on vehicle stability. Tests were made using the system without mass transfer, with mass transfer resulting from a subliming surface, and with mass transfer produced by blowing through a porous surface. The results of these tests, which were made in the FluiDyne Hypersonic Wind Tunnel at a nominal Mach number of 11, are described in this report. In addition to the data presented here, schlieren movies of several of the test runs were made.

## 2.0 FACILITY DESCRIPTION

The tests were performed in the FluiDyne Hypersonic Wind Tunnel at a nominal Mach number of 11. This is a free jet tunnel with a nozzle exit diameter of 20 inches. Air is stored at 5000 psi and is manually throttled to the desired stagnation pressure. The air is then heated by passing it through a zirconia cored brick bed storage heater which has been preheated by an oxygen-propane burner. A sketch of this tunnel is shown in Figure 1. This facility is more fully described in a booklet entitled, "Hypersonic Aerodynamic Studies," which is available from FluiDyne Engineering Corporation.

Stagnation pressure is measured with a test quality bourdon tube type gage and stagnation temperature with a Pt/Pt-10 Rh thermocouple located in the stilling chamber. Run times are on the order of 60 seconds. The model support system provides injection and retraction from the stream, axial translation, and pitching from -45° to +45° angle of attack.

During the first series of tests (ablating) in June 1966 and during the second series of tests (blowing) in January 1967, nozzle calibrations were performed. Results of the calibrations are as follows: the early calibration gave a variation of $\pm$ 0.8% from the mean Mach number over an eight inch test core; the latter calibration, after nozzle reassembly, gave a variation of $\pm$ 0.4%. The nozzle flow characteristics are shown in Figure 2 in terms of test section Mach numbers as a function of stagnation pressures and stagnation temperatures.

## 3.0 TEST MODEL AND INSTRUMENTATION DESCRIPTION

The dynamic stability coefficients for both ablating and blowing models of the same geometry were determined from the free oscillations on an air bearing support. In the case of the blowing model, additional instrumentation controlled the blowing so as to simulate ablation. The subsystems are the air bearing, the model position transducer, the blowing flow modulating needle valves, the pressure transducers, the mass transfer control, and the data acquisition system.

### 3.1 Dynamic Stability System

An assembly drawing of this system with two sectional views is shown in Figure 3A; details are shown in Figures 3B and 3C. A conical model mounted on an air bearing is free to oscillate in the vertical plane about its center of gravity. In the case of a blowing model as many as four porous skin sections may be employed.

The principal element of this system is the air bearing itself. The design of an air bearing which would operate satisfactorily and could still be entirely buried within a model was in itself a major problem which was significantly complicated by the need to "cross the bearing" with flow passages to the blowing compartments when blowing models were employed. Every effort was made to assure that the bearing oscillated with a minimum of viscous restraint and with no mechanical restraint. To accomplish this the flow passages were machined into the bearing and housing elements using what amounted to labyrinth seals at the intersections

to limit leakage to insignificant amounts, and no electrical or pneumatic leads were permitted to cross the bearing. This latter requirement meant that dynamic calibration of the system would be complicated, as described later, but the achievement of repeatable mechanical connections between the bearing rotor and stator components is not possible within the limits acceptable for this type of testing. The measurement of model position was accomplished within these restraints by the design and fabrication of a unique variable reluctance angle transducer.

Figures 4 and 5 show the bearing and model assembly installed in the wind tunnel.

The model is fastened to the air bearing rotor by means of the manifold and manifold clamp ring. The manifold or ycke is secured to the rotor and distributes the blowing air to the chambers. The angle of attack transducer body is secured to the air bearing housing while its armature is fastened to the yoke.

## 3.2 Mass Transfer System

This system modulates the model blowing as a function of the angle of attack and includes the elements that allow calibration so that instantaneous values of mass flow from each chamber can be deduced. Four needle valves modulate the gas flowing to the four model compartments. Rate of mass flow is inferred from four small pressure transducers located just downstream of the valves.

The four model compartments, or quadrants, are defined by the intersection of the horizontal plane through

the longitudinal axis and the vertical plane that contains the axis of rotation. Thus, we have fore and aft top and fore and aft bottom compartments which are shown in the sectionalized side view in Figure 3A.

The path of the blowing air from the needle valve to the chamber can be followed by reference to the two assembly views. Upon leaving the needle valve it passes the pressure transducer and is ducted to a groove on the bearing rotor which is ducted to the rotor end. The yoke or manifold connects the four rotor outlets to their respective model chambers.

The needle valves are actuated by hydraulic pressure to close and pneumatic to open. Lack of room for four return lines forced the use of a common pneumatic return. Coupled to each valve stem is a position feedback potentiometer.

The pressure transducers[1] are unique because of their small size which is about 1/4" O.D. by 1/4" long. They are of the capacitance type and are used in a special 100 k.c. carrier system which uses triaxial leads to circumvent changes in cable capacitance. The relationships between the mass flow through top and bottom chambers and the angle of attack are given in Figure 6. The phase lead shown as lambda can lag as well as lead. The fore and aft sections are independent of each other and can be set at different lambda values. The valve strokes can be changed

[1]Manufactured by Metrotech, Inc., Mountain View, Calif.

independently which allows adjustment of the mass flow ranges.

The functional elements of this system for one valve are shown in Figure 7. The needle valves are positioned by a closed loop servo system which is programmed by the lead-lag amplifier which has the angle of attack system output as its input. The hydraulic servo valves were mounted as close to the needle valves as possible. This meant installing them at the base of the model support strut. The hydraulic power supply was outside the test section. The model release mechanism allows release at $\pm 4$ and $\pm 8$ degrees. The Hidyne pressure transducers are mounted on the inner shell of the model with one side of their differential input in the blowing compartments. Their purpose is to get a correlation between chamber pressure and the pressure back at the Metrotech pressure transducers and the mass flow rate. The Hidyne lead wires are removed during a run. For dynamic calibration the signal generator simulates the model motion. The static flow calibration system contains two rotameter type flow meters, dehumidifiers, pressure gage, and two pressure regulators, which is sufficient equipment to obtain the mass flow rate at steady state conditions. Elements of the mass transfer control and calibration system are shown on Figures 8, 9, 10, and 11.

## 3.3 Models

Two types of models were used: one for the ablating series and another for the blowing series of runs. Both types used the same inner cone shown in Figure 3A.

### 3.3.1 Ablating Model

The requirement that this model have ablation over the whole surface, or ablate on the fore or aft of the CG only, leads to the design shown in Figure 12. The coated model, when initially coated, has the same dimensions as the blowing model. When only half the model is coated, the other half is replaced with a similar section of greater wall thickness to form a smooth juncture between the two halves. Two solid models are thus possible: one which has the same geometry as the blowing model and another which is smaller. Both of these solid models were tested.

The model geometry is as follows: (The "bare" figures are the dimensions of the small solid model and the "coated" figures are also the dimensions of the large solid model.)

A. Cone angle - 10°
B. $r_n/r_b = .166$
C. Axis of rotation = 56% of length from the nose
D. Open base
E. Length (bare) = 11.03", (coated) = 11.65"
F. Base diameter (bare) = 4.52", (coated) = 4.77"

Ablation models are shown on Figures 13, 14, and 15.

Two different materials were used in coating the models for ablation simulation testing. The materials used, paradichlorobenzene, $C_6H_4Cl_2$, and ammonium chloride, $NH_4Cl$, were selected because they each sublime at the

temperature levels reached and because they differed in mass loss rates. Ammonium chloride was applied to the nose and paradichlorobenzene to the conical section of the model.

The paradichlorobenzene was applied to the model in a liquid state by painting it onto the model after the model surface had been initially prepared by coating with Pliobond cement. When a sufficiently thick coating of ablation material had been achieved, the model was machined to the desired shape with the use of metal templates. The resulting surface was very smooth and had a waxy texture.

Prior to coating the nose with ammonium chloride it was given several coats of flat black paint and sprinkled with a medium coarse grit. This surface assured a good mechanical bond and protected the model from the corrosive effects of the ablation material. The finely ground ammonium chloride used was mixed with water to form a thick paste which was spread on the model. The coated model was baked until the moisture was removed and the ammonium chloride had hardened. The coatings were machined to shape after the model had cooled. Since the texture of the finished surface was fine grained and somewhat crumbly the model was handled as little as possible after coating.

The physical properties of the paradichlorobenzene and ammonium chloride can be obtained from References 4, 5, and 6. The density of the ablation material was less than theoretical due to the method of application. Measurements of the "as applied" material density have been

made and are: 1) paradichlorobenzene - 84.7 lbs/ft$^3$ and 2) ammonium chloride - 54.1 lbs/ft$^3$.

### 3.3.2 Blowing Model

The design objectives of this model were that the blowing rate decreases for increasing downstream stations and that the air volume between the outer porous skin and the inner shell be kept to a minimum. These are reflected in Figure 3A by the increasing porous skin thickness with increasing station and tapering of the blowing compartments to smaller widths away from the gas inlets. By keeping the compartment volumes small, their response is increased.

The model that was finally tested had a porous skin aft of the axis of rotation and a solid skin forward of it. The porous skin was Feltmetal[1] and, as assembled, allowed a mass flow rate of approximately .0004 lb/sec per compartment at a 14 psia internal comparment pressure and an external pressure of 6 Torr. The blowing model is shown on Figure 5.

## 3.4 Data Acquisition System

The requirements of this system are that it record the angle of attack of the model without phase lag and render its amplitude faithfully. Also, the output of the pressure transducers from which the mass flow rate is inferred must be measured with high fidelity. The model

---

[1]Registered trademark of the Huyck Corporation.

oscillating frequency varied from 2 to 3.5 cps, the value for any wind tunnel run being a function of the stagnation pressure for that run.

A multi-channel, light beam galvanometer, oscillograph was used to record all the data. The dynamic data were recorded with galvanometers that were 64% of critically damped and whose natural frequency was either 100 cps or 585 cps. The output/input amplitude ratio for both cases is one. The phase lag for the 100 cps case is less than 1° and for the 585 cps case is approximately 0°. The bandwidth of the transducer and electronic equipment "feeding" any galvanometer was greater than the galvanometer's. In short, the data acquisition system did not distort the data.

# 4.0 OPERATING PROCEDURES

## 4.1 Calibrations

The calibrations necessary are the bearing damping, model moment of inertia, angle of attack measuring system, static and dynamic mass transfer measuring systems, and weight loss/unit time of ablative material in the case of ablating models.

### 4.1.1 Bearing Damping

This is determined by clamping a gravity pendulum to the model. (See Figure 16.) This combination is allowed to oscillate in a chamber at ambient pressure and a fraction thereof. From these results it was concluded that ambient determination can be extrapolated to in vacuo conditions. A measure of damping, the logarithmic decrement is obtained from the recording of angle of attack.

### 4.1.2 Moment of Inertia

The moment of inertia of the oscillating mass was obtained in part by calculation and in part experimentally. Moment of inertia of the air bearing rotor, being of a simple shape and inaccessible, was calculated. A torsion pendulum was used to find the moment of inertia of the remaining mass, which was comprised of the model, manifold ring clamp and manifold. The frequency of oscillation of a bar of known moment of inertia was compared with the frequency of oscillation of unknown. The apparatus used is shown in Figure 17.

4.1.3 Angle of Attack

This measuring and recording system was proven with a precision inclinometer.

4.1.4 Mass Transfer

The calibration of the mass transfer measurement system was carried out in two steps. The primary standard employed was the rotameter which has a dynamic response which is too slow to be used to calibrate the system directly under dynamic conditions. The procedure followed was to use the rotameter to calibrate dynamic measuring devices (pressure transducers) under steady flow (static) conditions, after which a dynamic calibration was made using only the pressure transducers to determine the lag characteristics of the transducers located in the vicinity of the flow control valves (which are monitored during a test run) from the measurement of the pressure in the chambers by the chamber transducers (which are not monitored during a test run). These calibrations were made with the test cabin evacuated to simulate run pressure levels.

4.1.4.1 Static Calibration

This was done by metering the flow to one compartment, then to the other by opening and closing the appropriate needle valves. The pressure in the compartment (Hidyne transducer) was recorded for various mass flow rates. Only the aft top and bottom compartments were thus calibrated for this series of tests.

#### 4.1.4.2 Dynamic Calibration

Model oscillation, for purposes of blowing calibration, was simulated by driving the valves with a signal generator at the frequency expected during the run. Both the compartment pressure and the pressure at the needle valves were recorded. This provided a correlation of the pressure at the needle valve with the flow from the compartment through the previous static calibration.

Compartment cross-flow was checked by biasing one valve closed and observing its compartment pressure fluctuations as the other valve was modulated. Cross-flow was not significant.

## 4.2 Run Procedures

### 4.2.1 General

The operating procedure for a typical run was as follows. Prior to tunnel pressurization, the model was balanced and manually set to one of the four detent positions ($\pm 4°$ and $\pm 8°$). The tunnel was then closed and pressurization started. After reaching steady state $P_o$, the model was injected and the detent released. During the run, the time history of the model oscillation was recorded on an oscillograph. Prior to the flow breakdown the model was retracted from the stream.

### 4.2.2 Ablation Runs

For these runs the procedure was geared to obtaining the rate of sublimation of the coating. Time interval in the test flow was ascertained by recording model

support position. Upon retraction the model was cooled by a jet of air to reduce sublimation (see Figure 15).

For a typical run the air bearing damping was checked, the angle of attack measuring system calibrated, the model weighed and mounted, the run made, the model retracted and cooled as the tunnel was shut down, the test cabin opened, and the model weighed. Moment of inertia change during the run was not significant.

4.2.3 Blowing Runs

Blowing runs differed from ablation runs only with respect to the differing model setup and handling requirements. Thus, for blowing runs the principal unique requirements were to establish the blowing characteristics desired for the run, and to calibrate the various transducers involved with respect to the data acquisition system references and scales. This procedure, while simple in principle, requires extreme care in the coordination of the several subsystems involved.

Of the pressure transducers only the Hidyne were accessible for calibration, but from this the calibrations of the Metrotech transducers were inferred. Being differential-type transducers, pulling a vacuum to various levels on the side not in the model blowing compartment gave a calibration. Then by exhausting the test cabin and modulating the needle valve via the signal generator, a Hidyne-Metrotech correlation was achieved. Also, the maximum and minimum mass air flows from each compartment were set and matched by adjusting the supply pressure and valve stroke

and bias. Then the test cabin was opened and the Hidyne wiring removed.

Again the air bearing damping was checked, and the angle of attack measuring system calibrated prior to the run, as in the ablation runs.

# 5.0 DATA REDUCTION PROCEDURES AND RESULTS

## 5.1 General

There were 21 wind tunnel runs, subdivided as follows:

1. four runs with bare, non-ablating models intended to check the wind tunnel operating characteristics and establish the aerodynamic characteristics of the model configuration without ablation or blowing;
2. six ablation runs involving three different ablation configurations; and,
3. eleven runs with the blowing model of which one run was made without blowing, for reference purposes, and the other ten runs involved different phase shift angles between the blowing cycle and the model oscillation angle and different blowing intensities. All the blowing tests were made with the aft blowing configuration.

Details and dimensions of the various models are given in Section 3.3 and in Figures 3A and 12. Table 1 provides a summary of the runs with the bare and ablating models and Table 2 summarizes the runs with the blowing model. The runs marked with an asterisk were considered to provide valid data for the calculation of the stability derivatives and these runs were analyzed in detail. Data from the other runs were not considered valid for the reasons summarized in the Remarks column and discussed in Section 6.

information pertinent to a particular run and necessary for the data reduction is extracted from the following sources.

1. The run log, giving the tunnel operating conditions $P_o$, $T_o$, M, and the model geometric and physical characteristics.
2. The oscillograph traces for the full run chart including the pre-calibrations for the various transducers and the full-run, time-history of the model angle $\alpha$, test cabin static pressure p, the transducers monitoring $P_o$, $T_o$, or indicating model injection and ejection, and for the blowing models, the pressures in both top and bottom blowing chambers and the valve position transducer outputs.
3. The record of the bearing damping check carried out prior to and subsequent to the run; it gives the time history of the free oscillation of the angle $\alpha$ for the pendulum model arrangement.

A photographic record complemented the data for each run. The ablation runs were photographed by means of a schlieren sequence camera, capable of shooting up to 10 photographs during a 30-second run. Examples of the photographs obtained are shown on Figure 18. The instants of exposure are recorded by identifiable marks on the oscillograph recording chart. A continuous schlieren photographic record was made for all the blowing runs using a 16-millimeter Mitchell camera.

## 5.2 Test Section Flow Properties

The test section Mach number is calculated from the

tunnel calibration curve (Figure 2) at the run values of $P_o$ and $T_o$. Other test section flow properties are calculated from the flow tables in NACA Report 1135 with the Mach number as the independent variable and corrected for caloric imperfections by means of the following equations.

$$P = (P/P_o)(TP/P)_{P/P_o}(P_o)$$

$$q = (q/P_o)(TP/P)_{q/P_o}(P_o)$$

$$T = (T/T_o)(TP/P)_{T/T_o}(T_o)$$

$$\rho = \frac{P_o}{RT_o}\,\frac{(P/P_o)(TP/P)_{P/P_o}}{(T/T_o)(TP/P)_{T/T_o}}$$

$$V = 49.1\ M\sqrt{T}$$

where (TP/P) is the correction factor for caloric imperfection for the parameter identified by the related subscript. The factors used to correct for caloric imperfections are obtained from plots based on NACA Report 1135. Also, the test section Reynolds number per foot can be determined by a suitable plot based on the same reference.

## 5.3 Stability Derivatives

The static and dynamic stability derivatives, $C_{M_\alpha}$ and $C_{M_q} + C_{M_{\dot\alpha}}$ are calculated by the following procedure.

1. First, the run trace is carefully examined and any aspect of irregular behavior, particularly

as regards the cabin static pressure, is examined and the run intervals free from irregularities are selected.

2. The test section flow properties are obtained as indicated in 5.2.
3. The galvanometer deflections for $\alpha_{max}$ and $\alpha_{min}$ are read out from the oscillograph trace and the oscillation frequencies are calculated.
4. From the $\alpha$ calibration, the values of $\theta = 1/2(\alpha_{max} - \alpha_{min})$ are calculated and the time history curve, $\theta$ versus time, is plotted on semi-log paper.
5. Choosing suitable time intervals, $\Delta t$, on the $\theta$-time curve, a straight line tangent to the $\theta$ curve is drawn for each time increment and, from its intercepts, $\theta_1$ and $\theta_2$, at the ends of the interval, the quantity $\left[\ln(\theta_1/\theta_2)\right]/\Delta t$ is determined as an approximation to the derivative $\frac{d}{dt}\ln(\theta_1/\theta_2)$.
6. The total moment of inertia $I_{tot}$ is obtained by summation of the model moment of inertia, $I_{mod}$, and the bearing moment of inertia, $I_{bear}$.
7. The total damping moment, $M\dot{\theta}_{tot}$, is calculated from the equation

$$M\dot{\theta}_{tot} = -2(I_{tot})\,\frac{\ln(\theta_1/\theta_2)}{\Delta t}$$

8. The bearing damping moment, $M\dot{\theta}_{bear}$, is obtained directly from the bearing damping calibration and the value of the aerodynamic damping moment is calculated from the relation

$$M\dot{\theta}_{aero} = M\dot{\theta}_{tot} - M\dot{\theta}_{bear}$$

9. The static stability derivatives are calculated from the equation

$$C_{M_\alpha} = - \frac{I_{tot}\omega^2}{qSd} \quad \text{per radian}$$

10. The dynamic stability derivatives are calculated from the relation

$$C_{M_q} + C_{M_{\dot\alpha}} = \frac{M_{\dot\theta_{aero}}}{\frac{qSd^2}{2V}} \quad \text{per radian}$$

## 5.4 Mass Transfer Characteristics

### 5.4.1 Ablation

The ablation rate, $\dot m$, in lbs/sec, was determined by dividing the model weight loss during the run by the total run duration. In Table 1, the ablation intensity is also expressed by the non-dimensional quantity $\dot m/(\rho VS)$, using the free stream density and velocity and the model base area for reference purposes. It should be pointed out that neither $\dot m$ nor $\dot m/(\rho VS)$ gives a true indication of the local or even the average rate of ablation for different ablation configurations of the same model since the actual ablation area, $S_{Ab}$, will vary for the same base area. More realistic parameters for comparing different ablation geometries are $\dot m/(S_{Ab})$ and $\dot m/(\rho VS_{Ab})$.

The parameters $\dot m$ and $\dot m/(\rho VS)$ are used only for the purpose of determining the corresponding blowing rates for the same geometric configuration.

5.4.2 Blowing

One of the principal objectives of a blowing model is to simulate, as closely as possible, the mass transfer characteristics of the ablating body over the full cycle of oscillation. There are practical limitations of model design and construction which make exact simulation impossible to achieve. In the present model, the continuous transverse variation of ablation rate from a maximum at the windward side to a minimum at the leeward side is replaced by a stepwise change between a top and bottom chamber. The downstream variation in the ablating mass transfer rate, which will be different for the laminar and turbulent boundary layer cases, is approximated experimentally by increasing the skin thickness with increasing values of x. Attempts to measure the distribution of mass flow through the porous skin, or to check the actual porosity distribution of the skin by means of a hot wire anemometer, were unsatisfactory on account of the very small flow velocities. Tests of the blowing skin under water suggested the presence of pinholes and other irregularities; it has been assumed that such irregularities were randomly distributed and do not unduly vitiate the experimental observations.

The procedure for determining the timewise distribution of the rate of air mass blowing from each chamber for a particular run and its phase-shift with respect to the oscillation angle, $\alpha$, was as follows. A suitable time interval of 2 cycles of oscillation was selected from the run chart and divided into 32 equal intervals. The galvanometer traces from the Metrotech transducers recording the blowing chamber pressures were read off and converted to mass flow in lbs/sec (by use of the combined

static-dynamic calibrations described above) for each chamber. The mass flow was plotted along with the α-trace which, for all practical purposes, was a sine curve. The resulting mass flow distribution was not quite sinuscidal in shape, because of practical experimental limitations. A graphical procedure which, in effect, replaced the actual waveform by an appropriate sine wave with the same amplitude variation was adopted. This enabled an average phase-shift angle, assumed constant over the full cycle, to be determined. In general, the mass flow rates from the two chambers and the phase shift angles were not equal in spite of painstaking settings prior to the wind tunnel run. This result was due to the fact that it was not possible to set up the mass flow distributions and phase-shifts with the actual model in oscillation at the actual test frequency. Instead, an α-simulator was used for the initial settings, with the model itself stationary. The addition of a torsion pendulum to the system would eliminate this problem.

It is worth noting that a theoretical analysis of a blowing model may be employed to account for the effects of unequal blowing intensities or different phase angles on the static and dynamic stability derivatives.

# 6.0 ANALYSIS OF RESULTS AND CONCLUSIONS

## 6.1 General

As indicated in Section 5, the data from some runs had to be discarded. The main cause for invalidating a test run was a persistent cabin static pressure oscillation of the same frequency as that of the model oscillation; when this pressure fluctuation was appreciable, it appeared to drastically affect the calculated stability derivatives.

Another type of irregularity, observed with both the ablation and blowing models, was that of random, relatively large-amplitude, cabin static pressure pulses which had a strong, though localized, effect on the model, readily evident in the abrupt change in the $\alpha$-amplitude. Initially, it was feared that these static pressure transients vitiated the data for the entire run. However, careful examination of the records of a number of runs showed satisfactory consistency of the results calculated from the data for the intervening periods of steady cabin static pressure, particularly when these quiescent periods were of relatively long duration, of the order of 5 seconds or longer.

The plot of the time history for the run ($\theta$ versus $t$) on semilog paper was found to be a very convenient reference for an initial analysis of the run. The intervals of time during which the data are not influenced by static pressure transients (and thus are most suitable for reduction) are clearly shown.

## 6.2 Ablation Tests

### 6.2.1 Air Bearing Performance

The air bearing performed quite well for these runs, the bearing damping being small and generally repeatable. A plot of bearing damping is shown in Figure 19. The general level of damping appeared constant with amplitude and a value of $.05 \times 10^{-4}$ ft-lb/rad-sec was used for the data reduction of these runs. For comparison, the average damping calculated for the earlier, strut-mounted air bearing was $.22 \times 10^{-4}$ ft-lb/rad-sec.

It should be pointed out that the gravity pendulum used for the bearing damping checks allowed the system to oscillate at approximately 1 cps, whereas the frequency observed during the actual runs ranged between 2 and 3.5 cps.

### 6.2.2 Specific Remarks and Results of the Ablation Test Runs

Table 1 presents a convenient summary of the ablation test results, indicating the successful runs, and Figure 20 shows the time history, $\theta$ versus t, for these runs. The following remarks are pertinent to specific runs of Table 1.

Run 845, with the small bare model, involved only slight cabin pressure oscillations and no transient static pressure pulses. The model was released at 8 degrees, oscillated at a frequency of about 2.5 cps, and converged as expected. Table 3A lists some of the relevant characteristics for this run together with the calculated static and dynamic derivatives.

Run 846 involved the large model in the aft-ablation configuration. The model was released at 4 degrees and its oscillations diverged. The paradichlorobenzene sublimated at the rate of .006 lb/sec and slight oscillations were observed in the traces of the cabin static pressure. Details of this run and the calculated derivatives are listed in Table 3B.

Run 847 was essentially a repetition of Run 845. However, it displayed a number of random, static pressure pulses during the initial seconds of the run, after which period the cabin static pressure remained fairly steady and the subsequent data reduction yielded derivatives compatible with those of Run 845, thus supporting the assumption that valid results may be calculated from data away from the local static pressure disturbance. Table 3C presents the results obtained from this run.

Run 848 with the large, full-length-ablation model, and Runs 849 and 850 with the same model in the forward-ablation configuration, all displayed relatively large, persistent oscillations in the cabin static pressure, at the same frequency as the model oscillation, resulting in divergent oscillations for all three runs. It was suspected that the model was marginally large for the tunnel operation conditions of $P_o$ = 500 psia and $T_o$ = 3200°R.

Run 852, conducted with a bare model the same size as the ablating models, at $P_o$ = 500 psia and $T_o$ = 3100°R, confirmed the above suspicions. Appreciable oscillations in the cabin static pressure were observed and, contrary to the expected results, as demonstrated by Runs 845 and 847, the model oscillations diverged.

The remaining runs in this series, nambely 851, 853, and 854, were made at approximately $P_o$ = 1000 psia and $T_o$ = 2500°R and they all exhibited a steady cabin static pressure and produced valid run data. Test Runs 851 and 853 with the large, forward ablation configuration and release angles of 4 and 8 degrees respectively, displayed the same degree of convergence and approximately the same values for the derivatives as shown in Tables 3D and 3E. The results for the final test run in this series, Run 854 with the small, bare model released at 8 degrees, are given in Table 3F. The calculated values for the static and dynamic derivatives are compatible with the values obtained from Runs 845 and 847 at different wind tunnel operating conditions.

Figures 21 and 22 illustrate, for purposes of comparison, the calculated static and dynamic derivatives from all the valid runs in this series.

Figure 21 shows that, for the CG location of the present models, the variations in the static derivative, $C_{M_\alpha}$, with forward or aft ablation are relatively small, of the order of 10 percent of the original value of $C_{M_\alpha}$. This variation was stabilizing in the forward ablation configuration and destabilizing in the aft ablation configuration.

Figure 22 illustrates the variations in the dynamic derivative, $C_{M_q} + C_{M_{\dot\alpha}}$, produced as a result of forward or aft ablation. The variation in amplitude is roughly one order of magnitude larger than the original value and is stabilizing for the forward-ablation and destabilizing for the aft-ablation configurations.

Figure 23 illustrates a typical calibration curve of the $\alpha$-transducer taken from one of the ablation tests.

## 6.3 Blowing Tests

### 6.3.1 Air Bearing Performance

The air bearing performance, as indicated by the measured bearing damping moment, $M_{\dot{\theta}_{bear}}$, is illustrated in Figure 24 for the valid blowing test runs. Straight line approximations to the test values are also shown. For data reduction purposes, the value of the bearing damping for each test, at the relevant angle of oscillation, was read off the appropriate straight line. It is apparent that, even for the best damping case, associated with test Run 881, when the bearing damping moment was the least and very nearly constant for the whole range of oscillation angles, its numerical value of about $.4 \times 10^{-4}$ ft-lb/rad-sec was considerably larger than that of the ablation runs which averaged only $.05 \times 10^{-4}$ ft-lb/rad-sec.

All the bearing damping tests were carried out with a pendulum arrangement which oscillated the model at a frequency close to 1 cps; whereas the frequency of oscillation for the blowing tests centered around 2.5 cps.

With the larger bearing damping moments associated with the blowing model, there was no appreciable change in the measured bearing damping when the damping tests were carried out in the atmosphere or in an evacuated chamber.

The design demands on the air bearing for the multi-chamber, blowing model are far more stringent than those for the ablation model. In the latter, the air bearing essentially has only to provide a free support for the model oscillation; whereas in the former it has also to channel and control the blowing air to the respective chambers. Some difficulties with bearing heating and overloading were experienced when attempting to run the blowing tests at the wind tunnel conditions which had given consistently steady cabin static pressures for the ablation runs, namely $P_o$ = 1000 psia and $T_o$ = 2500°R.

### 6.3.2 Specific Remarks and Results of the Blowing Test Runs

Table 2 presents a summary of the 11 blowing test runs and indicates with an asterisk, the 7 runs which appeared to provide valid data suitable for detailed reduction and analysis.

The wind tunnel conditions chosen for Test Runs 874, 875, and 876 were those found to be the best for the ablation tests. The release angle of 4 degrees for these runs was chosen in anticipation of diverging oscillations for an aft blowing configuration with phase lag. However, these three runs showed very marked irregularities and had to be discarded. Run 874 exhibited the oscillating cabin static pressure described previously with rapidly decaying oscillations at a frequency of about 3.5 cps.

Run 875 was plagued with a delayed operation of the valve in the top chamber, an increasing model cavity pressure, and very rapidly decaying model oscillations.

A large, initial static pressure pulse occurred near the model release for Run 876 and it oscillated for barely two cycles. After each of the above three runs, the model became very hot and noticeably sluggish. Damping checks, performed immediately after the runs, indicated a considerable deterioration in the bearing performance, but the bearing damping characteristics returned to their earlier level after the model had returned to room temperature conditions.

All subsequent runs, namely 877 to 884, were made at around 500 psia for $P_o$, and 2400°R for $T_o$, and this alleviated the force and thermal loading on the bearing and model which remained relatively free and only moderately hot after these runs. The general level of the bearing damping crept up, however, with successive runs as shown in Figure 24.

In view of the fact (already noted for the ablation runs) that the wind tunnel operating conditions, in terms of diffuser performance, were somewhat marginal for the present size of the model, random static pressure pulses invariably occurred, sometimes in large number as indicated in Table 2 and Figure 25. This tended to restrict the valid data from some runs to shorter intervals and may be the cause of greater scatter in the calculated derivatives.

Table 2 lists the maximum and minimum blowing rates per chamber and the phase-shift angles $\lambda_1$ and $\lambda_2$ for the upper and lower chambers respectively, calculated by the method outlined in Section 5.4.2.

Improper cycling of the upper chamber valve sometimes occurred and it remained nearly fully open (Run 877) or fully closed (Run 882) and thus did not contribute to the derivative. The phase-shift angles for the upper and lower chambers differed markedly in the early runs. In the last two runs, however, as a result of working experience in setup and calibration, the phase-shift angles for the two chambers were remarkably close.

Tables 4A to 4G list the essential results of all the valid blowing runs.

The calculated values of the static stability derivative, $C_{M_\alpha}$, for the blowing runs are collected together and illustrated in Figure 26 which also shows the range of values of $C_{M_\alpha}$ for the non-ablating models to serve as reference. It will be noted that the range of variation in $C_{M_\alpha}$, due to blowing at the different rates and phase-shift angles used is relatively small, of the order of 10 percent. For the predominant cases of phase-lag, the effect of aft blowing is seen to be statically destabilizing.

All the calculated values of the dynamic stability derivative, $C_{M_q} + C_{M_{\dot\alpha}}$ for the blowing runs are collected together in Figure 27. The range of variation of $C_{M_q} + C_{M_{\dot\alpha}}$ for the bare, non-ablating model is also illustrated for reference purposes. In spite of the large scatter, evidenced by the results of some of the runs, and the very small rates of blowing in these runs, the following trends clearly emerge:

1. Run 878, involving negligible phase-shift, exhibits no appreciable change in the dynamic derivative.

2. Runs 879 and 882 produced the maximum positive dynamic derivatives; in other words, the effect of blowing was strongly destabilizing. These runs involved the largest phase-lag angles, although in Run 882, only the lower chamber cycled satisfactorily.
3. Run 883, the only run with large phase-lead angles, was the only run where the blowing increased the dynamic damping derivative.

## 6.4 Concluding Remarks

In any test program there are a great many factors which influence the precision of the test results. In a program in which the major effort has been the development of the test hardware and a test technique, an error analysis becomes impractical; such is the case here. The following commentary is therefore intended to give a basis for evaluating the potential capability of the test hardware and technique, rather than make any attempt to provide a classical error analysis of the component and system error characteristics.

The test facility itself, the Hypersonic Wind Tunnel, provides a reliable test stream in which to evaluate hypersonic flow characteristics. The run time of the order of 1 minute permits the use of instrumentation which has been widely accepted and which can be readily calibrated. One of the principal factors influencing the precision of coefficients determined by hypersonic testing is the problem of determination of the true flow Mach number, and thus dynamic pressure, to be used in reducing the data to coefficient form. In tests where large transverse and

axial gradients occur, the absolute values of coefficients can become meaningless. The use of a contoured nozzle in the FluiDyne wind tunnel minimizes the latter considerations such that the total probable variation in Mach number over the test core and the error in its average level can be expected to be within 1%. That this is the case is born out by the consistent results obtained from tests in this facility.

The special test apparatus has the same basic characteristic as the facility; the instrumentation used is of a type which has been generally widely accepted and, in this case more importantly, can be readily calibrated. In order to obtain a meaningful correlation between mass flow addition characteristics and resultant vehicle stability characteristics, it is necessary to know what the former are with an acceptable degree of precision. This is the basis for using a blowing system as opposed to employing natural ablation or sublimation of a coating, i.e., to achieve control over the experiment. The two principal parameters of interest are the blowing rate and its phase relationship to the body oscillation. Neither of these parameters can be precisely determined for the ablation or sublimation test. In the case of blowing tests, it is conceivable that these parameters might be measured directly; however, practical considerations generally require that the measurements be made indirectly during a run by use of pre-run calibrations and direct measurement of related parameters during a run. Mass flow calibrations, in effect, calibration of the flow through the porous skin, are made statically, i.e., with constant pressure differential across the wall. If pressure is measured upstream of

the chamber during a run, the chamber pressure must be inferred from calculations or a dynamic calibration made before the run. If the frequency at which the system is operating is high enough, both the amplitude decrement and phase shift between the pressure measuring point and the chamber can be substantial. Thus, although the flow path between the measuring point and the mass injection point may be short (such that the time required for a pressure pulse to traverse it is negligible), the important consideration is that of the flow process which occurs between these two points. For the system described here which operates at a frequency of several cycles per second, dynamic calibrations have demonstrated that the effect on amplitude and phase shift is negligible. (In the case where the system frequency is an order of magnitude larger, both of these factors can be expected to be significant, and extremely difficult if not, practically speaking, impossible to calibrate out.)

In the tests described herein it was found that even with the low frequency system and the provision of means for dynamic calibration, difficulties in pre-run setup and post-run data analysis were encountered. These were largely due to the fact that the dynamic calibration was achieved by use of a stationary model and a function generator to provide the input to the flow control system, or an oscillating model for which a gravity pendulum provided the driving force. In the latter case, the frequency of oscillation was only a fraction of that during wind tunnel testing; thus, both approaches only achieved partial simulation of the complete dynamic system. Any further testing should incorporate the use of a torsion pendulum as a device to oscillate the model at test frequencies with all systems operational to provide final dynamic calibrations and pre-run setup.

The single technical problem which gave rise to the largest number of practical difficulties in the experimental program was locating a suitable material for the porous surfaces of the blowing model. A suitable material for this purpose should have the following properties:

1. Fine-grained porosity so that when gas is blown through it, the length scale of nonuniformities in local mass flow rate will be small compared to the boundary layer thickness.
2. A porosity high enough that the permeability of practical thicknesses is high enough to pass the desired flow rates at chamber pressure low enough that the metering valves remain choked.
3. A porosity low enough that the blowing chamber pressure be high enough so that the volumetric flow rate between the control valves and the chamber is low enough to preclude choking between these points.
4. Machinability or formability so that an accurate cone frustum may be produced without closing the pores at the surface.
5. Sufficient mechanical strength to withstand the stresses developed by the internal (chamber) pressure.
6. Uniformity such that variations in porosity (averaged over areas small with respect to the total porous area) will be less than 20%.

During the course of a year, several different blowing surfaces were fabricated of sintered-metal products which were expected to have these characteristics; none

of the resulting surfaces were satisfactory when finally tested. The material which gave the best results and which was used in the test program reported here turned out to be very difficult to braze. An intermittent crack developed along the brazed longitudinal seams, which were located at +90° and -90° from the windward surface at positive angle of attack and undoubtedly a significant amount of the regulated blown air supply leaked out of these cracks instead of bleeding through the surface. The interaction of this leaked airflow with the external hypersonic flow could not cause much change in pitching moment, since the pressure loads thus generated would be at right angles to the pitching plane. It is thus probable that the actual mass transfer which was effective in changing the pitching moment and the pitch damping rate was much smaller than the values calculated and tabulated in Table 2. Also, as noted previously, there was evidence that the porosity distribution was quite nonuniform so that a significant amount of the regulated blown air supply may have been blown through the surface in small localized regions. This would also tend to reduce the effectiveness of the blown air in changing the aerodynamic pitching moment.

After these tests were completed, we located a third supplier whose sintered metal product appears to satisfy the practical requirements listed above. We plan to make bench tests of a model fabricated of this material to determine whether this is the case.

The limited experimental data obtained thus far and reported herein qualitatively confirm the results obtained from the theoretical analysis of the phenomenon (Reference 3). As mentioned previously, that portion

of Run 879 which was free of test cabin pressure fluctuations clearly demonstrated that the model was dynamically unstable with aft blowing with phase lag, as predicted by the analysis. Similarly, Run 883 showed conclusively that the pitch damping rate was greatly increased for aft blowing with phase lead. The changes in t e dynamic stability derivatives, $C_{M_q} + C_{M_{\dot{\alpha}}}$, for these runs was only about one-tenth of the change predicted by the analysis, however. A large part of this quantitative difference was undoubtedly the result of the leaks and nonuniformities in the porous skin described above.

REFERENCES

1. Grimes, J. H. Jr., and Casey, John J., "Influence of Ablation on the Dynamics of Slender Re-Entry Configurations," AIAA Journal of Spacecraft and Rockets, Vol. 2, No. 1, January-February 1965, pp. 106-108.

2. Holdhusen, J. S., Casey, John. J., and DeCoursin, David G., FluiDyne Engineering Corporation, "Some Considerations of the Effects of Mass Transfer on Aerodynamic Pitch Damping Coefficients," FluiDyne Interim Report 0414-2-15-65 on ARPA Order No. 576, ONR Contract Nonr 4624(00).

3. Ibrahim, S. K., and Holdhusen, J. S., FluiDyne Engineering Corporation, "Analysis of the Effects of Phased Cyclic Blowing on the Aerodynamic Pitching Moment Derivatives of Slender Cones in Hypersonic Flow," presented at a meeting of the Anti-Missile Research Advisory Council (AMRAC) April 1966.

4. Handbook of Chemistry and Physics, 42 edition.

5. Howell, Robert R., "An Experimental Study of the Behavior of Spheres Ablating Under Constant Aerodynamic Conditions," NASA TN D-1635.

6. Welker, Jean E., "Comparison of Theoretical and Experimental Values for the Effective Heat of Ablation of Ammonium Chloride," NASA TN D-553.

TABLE 1. SUMMARY OF ABLATION TEST RUNS

| Run | Configuration | $\theta$ Plane | $\theta_R$ | $P_\bullet$ psia | $T_o$, °R | $\dot{m}$ lbs/sec | $\dot{m}/\rho VS$ | f-cps | I ft-lbs-sec$^2$ | Remarks |
|---|---|---|---|---|---|---|---|---|---|---|
| 845* | Bare | V | 8 | 500 | 3100 | ---- | ---- | 2.5 | $69/^{-4}$ | Converging, slight cabin pressure fluctuation with model motion. |
| 846* | Aft Ablation | V | 4 | 500 | 3040 | .006 | .069 | 2.2 | $91/^{-4}$ | Diverging, slightly oscillating cabin pressure. |
| 847* | Bare | V | 8 | 500 | 3080 | ---- | ---- | 2.5 | $69/^{-4}$ | Converging, random bumps in cabin pressure. |
| 848 | All PDB | H | 8 | 500 | 3100 | .007 | .086 | 2.1 | $89/^{-4}$ | Diverging, oscillating cabin pressure. |
| 849 | Fwd Ablation | V | 8 | 505 | 3335 | .003 | .041 | 2.2 | $83/^{-4}$ | Diverging, oscillating cabin pressure, increasing cavity pressure. |
| 850 | Fwd Ablation | H | 8 | 505 | 3225 | .003 | .040 | 2.1 | $84/^{-4}$ | Diverging, oscillating cabin pressure, increasing cavity pressure. |
| 851* | Fwd Ablation | V | 4 | 995 | 2550 | .002 | .015 | 3.5 | $83/^{-4}$ | Converging, steady cabin pressure. |
| 852 | Bare | V | 8 | 500 | 3100 | ---- | ---- | 2.5 | $87/^{-4}$ | Diverging, large bare model same size as ablating models oscillating cabin pressure. |
| 853* | Fwd Ablation | V | 8 | 995 | 2430 | .002 | .013 | 3.5 | $84/^{-4}$ | Converging, steady cabin pressure. |
| 854* | Bare | V | 8 | 990 | 2540 | ---- | ---- | 3.3 | $69/^{-4}$ | Converging, small bare model, steady cabin pressure. |

TABLE 2. SUMMARY OF BLOWING TEST RUNS

| Run | $\alpha_R$ | $P_o$ (psia) | $T_o$ (°R) | f (cps) | Blowing Rates $\dot{m}$ lb/sec/chamber x $10^3$ upper $\dot{m}_{max}$ | upper $\dot{m}_{min}$ | lower $\dot{m}_{max}$ | lower $\dot{m}_{min}$ | Phase Shift $\lambda_1$ upper | $\lambda_2$ lower | Remarks |
|---|---|---|---|---|---|---|---|---|---|---|---|
| 874 | 4° | 1000 | 2365 | 3.47 | ---- | ---- | ---- | ---- | ---- | ---- | Oscillating cabin static pressure. |
| 875 | 4° | 1010 | 2420 | 3.54 | ---- | ---- | ---- | ---- | ---- | ---- | Delayed operation of top valve increasing cavity pressure. |
| 876 | 4° | 1000 | 2475 | ---- | ---- | ---- | ---- | ---- | ---- | ---- | Large initial static pressure pulses. Poor bearing performance. |
| 877* | 8° | 500 | 2480 | 2.55 | .50 | .50 | .40 | .20 | ---- | -41° | Ten transient static pressure pulses in 37-second run with periods of steady cabin pressure. |
| 878* | 8° | 500 | 2420 | 2.47 | .484 | .145 | .123 | 0 | -4° | +1° | Eight transient static pressure pulses in 22-second run with intervening periods of fairly smooth operation. |
| 879* | 8° | 500 | 2540 | 2.55 | .286 | .093 | .440 | .150 | -48° | -39° | Sixteen transient pressure pulses in 30-second run period; divergent oscillations during steady periods. |
| 880 | 8° | 500 | 2460 | 2.55 | No Blowing | | | | ---- | ---- | Slightly oscillating cabin static pressure. No transient static pressure pulses. |
| 881* | 8° | 500 | 2425 | 2.43 | .438 | .150 | .471 | .156 | -27° | -18° | Four transient static pressure pulses in 42-second run, smooth operation in intervening periods. |

TABLE 2a. SUMMARY OF BLOWING TEST RUNS

| Run | $\alpha_R$ | $P_o$ (psia) | $T_o$ (°R) | f (cps) | Blowing Rates lb/sec/chamber x $10^3$ upper $\dot{m}_{max}$ | upper $\dot{m}_{min}$ | lower $\dot{m}_{max}$ | lower $\dot{m}_{min}$ | Phase Shift $\lambda_1$ upper | $\lambda_2$ lower | Remarks |
|---|---|---|---|---|---|---|---|---|---|---|---|
| 882* | 4° | 520 | 2415 | 2.60 | .080 | .045 | .530 | .235 | ---- | -45° | Eleven transient static pressure pulses in 28-second run, low mass flow rate from upper chamber. |
| 883* | 8° | 500 | 2300 | 2.60 | .427 | .138 | .505 | .175 | +33° | +35° | Four transient static pressure pulses in 27-second run, satisfactory operation with phase lead in intervening steady periods. |
| 884* | 8° | 510 | 2420 | 2.47 | .467 | .050 | .397 | .164 | -26° | -25° | Six transient static pressure pulses in 29-second run, steady cabin static pressure in intervening periods. |

TABLE 3a. ABLATION RUN DATA TABULATIONS

Run 845, Configuration: Small, Bare Model

$I_{tot} = 68.94 \times 10^{-4}$ ft-lb-sec$^2$ $I_{model} = 68.88 \times 10^{-4}$ ft-lb-sec$^2$

$P_o = 500$ psia $T_o = 3100°R$ $M = 10.89$ $Re/ft = .183 \times 10^6$

| Time From Release (sec) | $\theta$ (degree) | f (cps) | $M_{\dot{\theta}_{tot}} \times 10^4$ (ft-lb/rad-sec) | $M_{\dot{\theta}_{bear}} \times 10^4$ (ft-lb/rad-sec) | $M_{\dot{\theta}_{aero}} \times 10^4$ (ft-lb/rad-sec) | $C_{M_q} + C_{M_{\dot{\alpha}}}$ (radian$^{-1}$) | $C_{M_\alpha}$ (radian$^{-1}$) |
|---|---|---|---|---|---|---|---|
| 7.6 | 7.01 | 2.42 | -1.626 | -.050 | -1.576 | -1.933 | -.587 |
| 9.6 | 6.82 | 2.45 | -1.528 | -.050 | -1.478 | -1.813 | -.599 |
| 11.6 | 6.65 | 2.46 | -1.368 | -.050 | -1.318 | -1.617 | -.606 |
| 13.6 | 6.54 | 2.48 | -1.368 | -.050 | -1.318 | -1.617 | -.614 |
| 14.6 | 6.48 | 2.48 | -1.260 | -.050 | -1.210 | -1.484 | -.614 |
| 16.6 | 6.41 | 2.48 | -1.260 | -.050 | -1.210 | -1.484 | -.617 |
| 17.6 | 6.33 | 2.48 | -1.185 | -.050 | -1.135 | -1.392 | -.612 |
| 19.6 | 6.21 | 2.49 | -1.185 | -.050 | -1.135 | -1.392 | -.618 |
| 20.6 | 6.17 | 2.49 | -1.073 | -.050 | -1.023 | -1.255 | -.618 |

TABLE 3b. ABLATION RUN DATA TABULATIONS

Run 846, Configuration: Aft Ablation Model

$I_{tot} = 90.68 \times 10^{-4}$ ft-lb-sec$^2$ $I_{model} = 90.62 \times 10^{-4}$ ft-lb-sec$^2$

$P_o = 500$ psia $T_o = 3040°R$ $M = 10.92$ $Re/ft = .188 \times 10^6$

| Time from Release (sec) | $\theta$ (degree) | f (cps) | $M_{\dot{\theta}_{tot}} \times 10^4$ (ft-lb/rad-sec) | $M_{\dot{\theta}_{bear}} \times 10^4$ (ft-lb/rad-sec) | $M_{\dot{\theta}_{aero}} \times 10^4$ (ft-lb/rad-sec) | $C_{M_q} + C_{M_{\dot{\alpha}}}$ (radian$^{-1}$) | $C_{M_\alpha}$ (radian$^{-1}$) |
|---|---|---|---|---|---|---|---|
| 0 | 3.91 | 2.26 | 5.559 | -.050 | 5.609 | 5.491 | -.572 |
| 1 | 4.06 | 2.24 | 6.139 | -.050 | 6.189 | 6.059 | -.560 |
| 2 | 4.15 | 2.24 | 6.465 | -.050 | 6.515 | 6.378 | -.560 |
| 3 | 4.37 | 2.24 | 6.964 | -.050 | 7.014 | 6.867 | -.560 |
| 4 | 4.53 | 2.24 | 7.263 | -.050 | 7.313 | 7.159 | -.560 |
| 5 | 4.76 | 2.24 | 7.735 | -.050 | 7.785 | 7.622 | -.560 |
| 6 | 4.95 | 2.24 | 8.043 | -.050 | 8.093 | 7.923 | -.560 |
| 7 | 5.15 | 2.22 | 8.379 | -.050 | 8.429 | 8.252 | -.553 |
| 8 | 5.40 | 2.21 | 8.633 | -.050 | 8.683 | 8.501 | -.547 |
| 9 | 5.67 | 2.21 | 8.869 | -.050 | 8.919 | 8.732 | -.547 |
| 10 | 5.94 | 2.162 | 9.114 | -.050 | 9.164 | 8.972 | -.524 |

TABLE 3c. ABLATION RUN DATA TABULATIONS

Run 847, Configuration: Small, Bare Model

$I_{tot} = 68.94 \times 10^{-4}$ ft-lb-sec$^2$ $I_{model} = 68.88 \times 10^{-4}$ ft-lb-sec$^2$

$P_o = 500$ psia $T_o = 3080°R$ $M = 10.90$ $Re/ft = .185 \times 10^6$

| Time from Release (sec) | $\theta$ (degree) | f (cps) | $M_{\dot{\theta}_{tot}} \times 10^4$ (ft-lb/rad-sec) | $M_{\dot{\theta}_{bear}} \times 10^4$ (ft-lb/rad-sec) | $M_{\dot{\theta}_{aero}} \times 10^4$ (ft-lb/rad-sec) | $C_{M_q} + C_{M_{\dot{\alpha}}}$ (radian$^{-1}$) | $C_{M_\alpha}$ (radian$^{-1}$) |
|---|---|---|---|---|---|---|---|
| 6 | 4.38 | 1.57 | -1.019 | -.050 | -.969 | -1.185 | -.649 |
| 8 | 4.32 | 1.57 | -1.019 | -.050 | -.969 | -1.185 | -.649 |
| 10 | 4.26 | 1.57 | -1.019 | -.050 | -.969 | -1.185 | -.649 |
| 12 | 4.14 | 1.57 | -1.019 | -.050 | -.969 | -1.185 | -.649 |
| 14 | 4.09 | 1.56 | -1.019 | -.050 | -.969 | -1.185 | -.658 |
| 16 | 4.08 | 1.56 | -1.019 | -.050 | -.969 | -1.185 | -.658 |
| 18 | 4.05 | 1.56 | -1.019 | -.050 | -.969 | -1.185 | -.658 |
| 20 | 3.96 | 1.56 | -1.019 | -.050 | -.969 | -1.185 | -.658 |

TABLE 3d. ABLATION RUN DATA TABULATIONS

Run 851, Configuration: Forward Ablation Model

$I_{tot} = 82.80 \times 10^{-4}$ ft-lb-sec$^2$ $I_{model} = 82.74 \times 10^{-4}$ ft-lb-sec$^2$

$P_o = 995$ psia $T_o = 2550°R$ $M = 11.20$ $Re/ft = .500 \times 10^6$

| Time from Release (sec) | $\theta$ (degree) | f (cps) | $M_{\dot{\theta}_{tot}} \times 10^4$ (ft-lb/rad-sec) | $M_{\dot{\delta}_{bear}} \times 10^4$ (ft-lb/rad-sec) | $M_{\dot{\theta}_{aero}} \times 10^4$ (ft-lb/rad-sec) | $C_{M_q} + C_{M_{\dot{\alpha}}}$ (radian$^{-1}$) | $C_{M_\alpha}$ (radian$^{-1}$) |
|---|---|---|---|---|---|---|---|
| 1.0 | 3.16 | 3.48 | -15.841 | -.050 | -15.791 | -7.46 | -.659 |
| 2.0 | 2.86 | 3.48 | -15.988 | -.050 | -15.938 | -7.53 | -.659 |
| 4.0 | 2.37 | 3.48 | -16.342 | -.050 | -16.292 | -7.70 | -.659 |
| 6.0 | 1.97 | 3.48 | -16.908 | -.050 | -16.858 | -7.97 | -.659 |
| 8.0 | 1.53 | 3.48 | -16.977 | -.050 | -16.927 | -8.00 | -.659 |
| 10.0 | 1.30 | 3.48 | -17.370 | -.050 | -17.320 | -8.19 | -.659 |
| 12.0 | 1.04 | 3.48 | -17.370 | -.050 | -17.320 | -8.19 | -.659 |

TABLE 3e. ABLATION RUN DATA TABULATIONS

RUN 853, Configuration: Forward Ablation Model

$I_{tot} = 84.28 \times 10^{-4}$ ft-lb-sec$^2$ $I_{model} = 84.22 \times 10^{-4}$ ft-lb-sec$^2$

$P_o = 995$ psia $T_o = 2430°R$ $M = 11.25$ $Re/ft = .537 \times 10^6$

| Time from Release (sec) | $\theta$ (degree) | f (cps) | $M_{\dot{\theta}_{tot}} \times 10^4$ (ft-lb/rad-sec) | $M_{\dot{\theta}_{bear}} \times 10^4$ (ft-lb/rad-sec) | $M_{\dot{\theta}_{aero}} \times 10^4$ (ft-lb/rad-sec) | $C_{M_q} + C_{M_{\dot{\alpha}}}$ (radian$^{-1}$) | $C_{M_\alpha}$ (radian$^{-1}$) |
|---|---|---|---|---|---|---|---|
| 2.0 | 5.81 | 3.31 | -15.223 | -.050 | -15.173 | -7.057 | -.613 |
| 4.0 | 4.86 | 3.44 | -15.223 | -.050 | -15.173 | -7.057 | -.663 |
| 6.0 | 4.05 | 3.45 | -15.223 | -.050 | -15.173 | -7.057 | -.666 |
| 8.0 | 3.36 | 3.51 | -15.937 | -.050 | -15.887 | -7.389 | -.690 |
| 10.0 | 2.78 | 3.51 | -16.208 | -.050 | -16.158 | -7.515 | -.690 |
| 12.0 | 2.28 | 3.51 | -16.600 | -.050 | -16.550 | -7.698 | -.690 |
| 14.0 | 1.87 | 3.51 | -16.745 | -.050 | -16.695 | -7.765 | -.690 |
| 16.0 | 1.54 | 3.51 | -16.745 | -.050 | -16.695 | -7.765 | -.690 |
| 18.0 | 1.24 | 3.51 | -19.172 | -.050 | -19.122 | -8.894 | -.690 |

TABLE 3f. ABLATION RUN DATA TABULATIONS

Run 854, Configuration: Small Bare Model

$I_{tot} = 68.94 \times 10^{-4}$ ft-lb-sec$^2$ $I_{model} = 68.88 \times 10^{-4}$ ft-lb-sec$^2$

$P_o = 990$ psia $T_o = 2540°R$ $M = 11.20$ $Re/ft = .500 \times 10^6$

| Time from Release (sec) | $\theta$ (degree) | f (cps) | $M_{\dot{\theta}_{tot}} \times 10^4$ (ft-lb/rad-sec) | $M_{\dot{\theta}_{bear}} \times 10^4$ (ft-lb/rad-sec) | $M_{\dot{\theta}_{aero}} \times 10^4$ (ft-lb/rad-sec) | $C_{M_q} + C_{M_{\dot{\alpha}}}$ (radian$^{-1}$) | $C_{M_\alpha}$ (radian$^{-1}$) |
|---|---|---|---|---|---|---|---|
| 1.4 | 7.00 | 3.27 | -3.646 | -.050 | -3.596 | -2.114 | -.568 |
| 3.4 | 6.61 | 3.31 | -3.646 | -.050 | -3.596 | -2.114 | -.583 |
| 5.4 | 6.32 | 3.31 | -3.646 | -.050 | -3.596 | -2.114 | -.583 |
| 7.4 | 5.95 | 3.32 | -3.646 | -.050 | -3.596 | -2.114 | -.586 |
| 9.4 | 5.65 | 3.32 | -3.168 | -.050 | -3.118 | -1.833 | -.586 |
| 11.4 | 5.43 | 3.32 | -2.531 | -.050 | -2.481 | -1.459 | -.586 |
| 13.4 | 5.24 | 3.39 | -2.531 | -.050 | -2.481 | -1.459 | -.593 |
| 15.4 | 5.11 | 3.36 | -2.723 | -.050 | -2.673 | -1.571 | -.600 |
| 17.4 | 4.87 | 3.37 | -3.075 | -.050 | -3.025 | -1.778 | -.603 |
| 19.4 | 4.58 | 3.38 | -3.588 | -.050 | -3.538 | -2.080 | -.606 |

TABLE 4a. BLOWING RUN DATA TABULATIONS

Run 877, Configuration: Aft Blowing, $\lambda_2 = -41°$

$I_{tot} = 61.28 \times 10^{-4}$ ft-lb-sec$^2$ $I_{model} = 61.22 \times 10^{-4}$ ft-lb-sec$^2$

$P_o = 500$ psia $T_o = 2480°R$ $M = 11.08$ $Re/ft = .273 \times 10^6$

| Time from Release (sec) | $\theta$ (degree) | f (cps) | $M_{\dot{\theta}_{tot}} \times 10^4$ (ft-lb/rad-sec) | $M_{\dot{\theta}_{bear}} \times 10^4$ (ft-lb/rad-sec) | $M_{\dot{\theta}_{aero}} \times 10^4$ (ft-lb/rad-sec) | $C_{M_q} + C_{M_{\dot{\alpha}}}$ (radian$^{-1}$) | $C_{M_\alpha}$ (radian$^{-1}$) |
|---|---|---|---|---|---|---|---|
| 3.0 | 3.75 | 2.55 | -1.004 | -.720 | -.284 | -.306 | -.574 |
| 4.0 | 3.71 | 2.55 | -1.004 | -.720 | -.284 | -.306 | -.574 |
| 5.0 | 3.67 | 2.57 | -1.004 | -.720 | -.284 | -.306 | -.582 |
| 7.0 | 3.63 | 2.57 | -1.004 | -.720 | -.284 | -.306 | -.582 |
| 8.0 | 3.63 | 2.55 | -1.004 | -.720 | -.284 | -.306 | -.574 |
| 10.0 | 3.54 | 2.56 | -1.004 | -.720 | -.284 | -.306 | -.579 |
| 17.0 | 2.76 | 2.56 | -2.444 | -.720 | -1.724 | -1.857 | -.579 |
| 18.0 | 2.68 | 2.56 | -2.444 | -.720 | -1.724 | -1.857 | -.579 |
| 19.0 | 2.66 | 2.56 | -2.444 | -.720 | -1.724 | -1.857 | -.579 |
| 20.0 | 2.61 | 2.56 | -2.444 | -.720 | -1.724 | -1.857 | -.579 |

TABLE 4b. BLOWING RUN DATA TABULATIONS

Run 878, Configuration: Aft Blowing, $\lambda_1 = -4$, $\lambda_2 = +1$

$I_{tot} = 61.28 \times 10^{-4}$ ft-lb-sec$^2$ $I_{model} = 61.22 \times 10^{-4}$ ft-lb-sec$^2$

$P_o = 500$ psia $T_o = 2420°R$ $M = 11.11$ $Re/ft = .285 \times 10^6$

| Time from Release (sec) | $\theta$ (degree) | f (cps) | $M_{\dot{\theta}_{tot}} \times 10^4$ (ft-lb/rad-sec) | $M_{\dot{\theta}_{bear}} \times 10^4$ (ft-lb/rad-sec) | $M_{\dot{\theta}_{aero}} \times 10^4$ (ft-lb/rad-sec) | $C_{M_q} + C_{M_\alpha}$ (radian$^{-1}$) | $C_{M_\alpha}$ (radian$^{-1}$) |
|---|---|---|---|---|---|---|---|
| 0 | 6.12 | ---- | -1.775 | -.505 | -1.270 | -1.357 | ----- |
| 1 | 6.06 | 2.46 | -1.775 | -.505 | -1.270 | -1.357 | -.537 |
| 2 | 5.95 | 2.47 | -1.775 | -.505 | -1.270 | -1.357 | -.543 |
| 3 | 5.88 | ---- | -1.775 | -.505 | -1.270 | -1.357 | ----- |
| 4 | 5.75 | 2.47 | -1.673 | -.505 | -1.168 | -1.248 | -.543 |
| 5 | 5.71 | 2.49 | -1.673 | -.505 | -1.168 | -1.248 | -.550 |
| 6 | 5.64 | 2.47 | -1.673 | -.505 | -1.168 | -1.248 | -.543 |
| 7 | 5.52 | ---- | -1.673 | -.505 | -1.168 | -1.248 | ----- |

TABLE 4c. BLOWING RUN DATA TABULATIONS

Run 879, Configuration: Aft Blowing, $\lambda_1 = -48°$, $\lambda_2 = -39°$

$I_{tot} = 61.28 \times 10^{-4}$ ft-lb-sec$^2$ $I_{model} = 61.22 \times 10^{-4}$ ft-lb-sec$^2$

$P_o = 500$ psia $T_o = 2540°R$ $M = 11.06$ $Re/ft = .263 \times 10^6$

| Time from Release (sec) | $\theta$ (degree) | f (cps) | $M_{\dot{\theta}_{tot}} \times 10^4$ (ft-lb/rad-sec) | $M_{\dot{\theta}_{bear}} \times 10^4$ (ft-lb/rad-sec) | $M_{\dot{\theta}_{aero}} \times 10^4$ (ft-lb/rad-sec) | $C_{M_q} + C_{M_{\dot{\alpha}}}$ (radian$^{-1}$) | $C_{M_\alpha}$ (radian$^{-1}$) |
|---|---|---|---|---|---|---|---|
| 7 | 4.10 | 2.55 | 3.241 | -.385 | 3.626 | 3.949 | -.575 |
| 8 | 4.14 | 2.55 | 3.241 | -.385 | 3.626 | 3.949 | -.575 |
| 9 | 4.26 | 2.55 | 3.241 | -.385 | 3.626 | 3.949 | -.575 |
| 10 | 4.36 | 2.55 | 3.241 | -.385 | 3.626 | 3.949 | -.575 |
| 11 | 4.48 | 2.55 | 3.241 | -.385 | 3.626 | 3.949 | -.575 |
| 12 | 3.98 | 2.55 | 3.183 | -.385 | 3.568 | 3.886 | -.575 |
| 13 | 4.10 | 2.55 | 3.183 | -.385 | 3.568 | 3.886 | -.575 |
| 15 | 4.28 | 2.55 | 3.183 | -.385 | 3.568 | 3.886 | -.575 |
| 16 | 4.43 | 2.55 | 3.183 | -.385 | 3.568 | 3.886 | -.575 |

TABLE 4d. BLOWING RUN DATA TABULATIONS

Run 881, Configuration: Aft Blowing, $\lambda_1 = -27°$, $\lambda_2 = -18°$

$I_{tot} = 61.28 \times 10^{-4}$ ft-lb-sec$^2$ $I_{model} = 61.22 \times 10^{-4}$ ft-lb-sec$^2$

$P_o = 500$ psia $T_o = 2425°R$ $M = 11.10$ $Re/ft = .283 \times 10^{}$

| Time from Release (sec) | $\theta$ (degree) | f (cps) | $M_{\dot{\theta}_{tot}} \times 10^4$ (ft-lb/rad-sec) | $M_{\dot{\theta}_{bear}} \times 10^4$ (ft-lb/rad-sec) | $M_{\dot{\theta}_{aero}} \times 10^4$ (ft-lb/rad-sec) | $C_{M_q} + C_{M_{\dot{\alpha}}}$ (radian$^{-1}$) | $C_{M_\alpha}$ (radian$^{-1}$) |
|---|---|---|---|---|---|---|---|
| 1.0 | 7.03 | 2.42 | -1.812 | -.395 | -1.417 | -1.510 | -.520 |
| 3.0 | 6.82 | 2.42 | -2.248 | -.395 | -1.853 | -1.975 | -.520 |
| 5.0 | 6.56 | 2.41 | -2.703 | -.395 | -2.308 | -2.459 | -.514 |
| 7.0 | 6.75 | 2.42 | -1.812 | -.395 | -1.417 | -1.510 | -.520 |
| 9.0 | 6.62 | 2.44 | -.483 | -.395 | -.088 | -.094 | -.527 |
| 11.0 | 6.59 | 2.44 | -.243 | -.395 | +.152 | +.162 | -.527 |
| 13.0 | 6.56 | 2.45 | 0 | -.395 | +.395 | +.421 | -.534 |
| 15.0 | 5.82 | 2.50 | -.389 | -.395 | +.006 | +.006 | -.554 |
| 17.0 | 5.79 | 2.49 | -.634 | -.395 | -.239 | -.255 | -.547 |
| 19.0 | 5.68 | 2.47 | -.722 | -.395 | -.327 | -.348 | -.540 |

TABLE 4e. BLOWING RUN DATA TABULATIONS

Run 882, Configuration: Aft Blowing, $\lambda_2 = -45°$

$I_{tot} = 61.28 \times 10^{-4}$ ft-lb-sec$^2$ $I_{model} = 61.22 \times 10^{-4}$ ft-lb-sec$^2$

$P_o = 520$ psia $T_o = 2415°R$ $M = 11.11$ $Re/ft = .296 \times 10^6$

| Time from Release (sec) | $\theta$ (degree) | f (cps) | $M_{\dot{\theta}_{tot}} \times 10^4$ (ft-lb/rad-sec) | $M_{\dot{\alpha}_{bear}} \times 10^4$ (ft-lb/rad-sec) | $M_{\dot{\theta}_{aero}} \times 10^4$ (ft-lb/rad-sec) | $C_{M_q} + C_{M_{\dot{\alpha}}}$ (radian$^{-1}$) | $C_{M_\alpha}$ (radian$^{-1}$) |
|---|---|---|---|---|---|---|---|
| 0 | 3.40 | 2.57 | 0 | -.720 | .720 | .738 | -.565 |
| 2 | 3.40 | 2.62 | .716 | -.720 | 1.436 | 1.472 | -.588 |
| 4 | 3.52 | 2.62 | 2.905 | -.720 | 3.625 | 3.717 | -.588 |
| 6 | 2.82 | 2.66 | 3.455 | -.720 | 4.175 | 4.281 | -.604 |
| 7 | 2.92 | 2.62 | 3.455 | -.720 | 4.175 | 4.281 | -.588 |
| 8 | 2.98 | 2.59 | 3.455 | -.720 | 4.175 | 4.281 | -.572 |
| 10 | 2.39 | 2.68 | 2.679 | -.720 | 3.399 | 3.485 | -.612 |
| 11 | 2.44 | 2.68 | 3.093 | -.720 | 3.793 | 3.889 | -.612 |
| 12 | 2.51 | 2.64 | 3.607 | -.720 | 4.327 | 4.437 | -.596 |
| 13 | 2.63 | 2.62 | 4.363 | -.720 | 5.083 | 5.212 | -.589 |

TABLE 4f. BLOWING RUN DATA TABULATIONS

Run 883, Configuration: Aft Blowing, $\lambda_1 = +33°$, $\lambda_2 = +35°$

$I_{tot} = 61.28 \times 10^{-4}$ ft-lb-sec$^2$ $I_{model} = 61.22 \times 10^{-4}$ ft-lb-sec$^2$

$P_o = 500$ psia $T_o = 2300°R$ $M = 11.16$ $Re/ft = .310 \times 10^6$

| Time from Release (sec) | $\theta$ (degree) | f (cps) | $M_{\dot{\theta}_{tot}} \times 10^4$ (ft-lb/rad-sec) | $M_{\dot{\theta}_{bear}} \times 10^4$ (ft-lb/rad-sec) | $M_{\dot{\theta}_{aero}} \times 10^4$ (ft-lb/rad-sec) | $C_{M_q} + C_{M_{\dot{\alpha}}}$ (radian$^{-1}$) | $C_{M_\alpha}$ (radian$^{-1}$) |
|---|---|---|---|---|---|---|---|
| 1.0 | 6.63 | 2.50 | -8.576 | -.863 | -7.713 | -8.075 | -.558 |
| 2.0 | 6.23 | 2.51 | -6.384 | -.863 | -5.521 | -5.780 | -.566 |
| 4.0 | 5.74 | 2.51 | -4.199 | -.863 | -3.336 | -3.492 | -.566 |
| 6.0 | 4.86 | 2.56 | -7.736 | -.908 | -6.878 | -7.201 | -.588 |
| 8.0 | 4.36 | 2.60 | -5.589 | -.908 | -4.681 | -4.901 | -.604 |
| 9.0 | 3.70 | 2.63 | -6.636 | -.953 | -5.683 | -5.950 | -.620 |
| 11.0 | 3.36 | 2.63 | -5.779 | -.953 | -4.826 | -5.052 | -.620 |
| 13.0 | 3.06 | 2.63 | -5.190 | -.953 | -4.237 | -4.436 | -.620 |
| 15.0 | 2.80 | 2.63 | -4.859 | -.953 | -3.906 | -4.089 | -.620 |
| 17.0 | 2.65 | 2.63 | -4.552 | -.953 | -3.599 | -3.768 | -.620 |
| 19.0 | 2.43 | 2.63 | -4.278 | -.953 | -3.325 | -3.481 | -.620 |

TABLE 4g. BLOWING RUN DATA TABULATIONS

Run 884, Configuration: Aft Blowing, $\lambda_1 = -26°$, $\lambda_2 = -25°$

$I_{tot} = 61.28 \times 10^{-4}$ ft-lb-sec$^2$ $I_{model} = 61.22 \times 10^{-4}$ ft-lb-sec$^2$

$P_o = 510$ psia $T_o = 2420°R$ $M = 11.11$ $Re/ft = .291 \times 10^6$

| Time from Release (sec) | $\theta$ (degree) | f (cps) | $M_{\dot{\theta}_{tot}} \times 10^4$ (ft-lb/rad-sec) | $M_{\dot{\theta}_{bear}} \times 10^4$ (ft-lb/rad-sec) | $M_{\dot{\theta}_{aero}} \times 10^4$ (ft-lb/rad-sec) | $C_{M_q} + C_{M_{\dot{\alpha}}}$ (radian$^{-1}$) | $C_{M_\alpha}$ (radian$^{-1}$) |
|---|---|---|---|---|---|---|---|
| 2 | 6.58 | 2.47 | -.229 | -.950 | .721 | .755 | -.530 |
| 4 | 6.54 | 2.48 | -.229 | -.950 | .721 | .755 | -.537 |
| 6 | 6.63 | 2.48 | -.229 | -.950 | .721 | .755 | -.537 |
| 8 | 6.46 | 2.48 | -.381 | -.950 | .569 | .596 | -.537 |
| 10 | 6.44 | 2.48 | -.550 | -.950 | .400 | .419 | -.537 |
| 12 | 6.35 | 2.48 | -.857 | -.950 | .093 | .097 | -.537 |
| 14 | 6.23 | 2.48 | -1.148 | -.950 | -.198 | -.207 | -.537 |
| 16 | 6.13 | 2.47 | -1.308 | -.950 | -.358 | -.375 | -.530 |
| 18 | 6.02 | 2.48 | -1.479 | -.950 | -.529 | -.554 | -.537 |

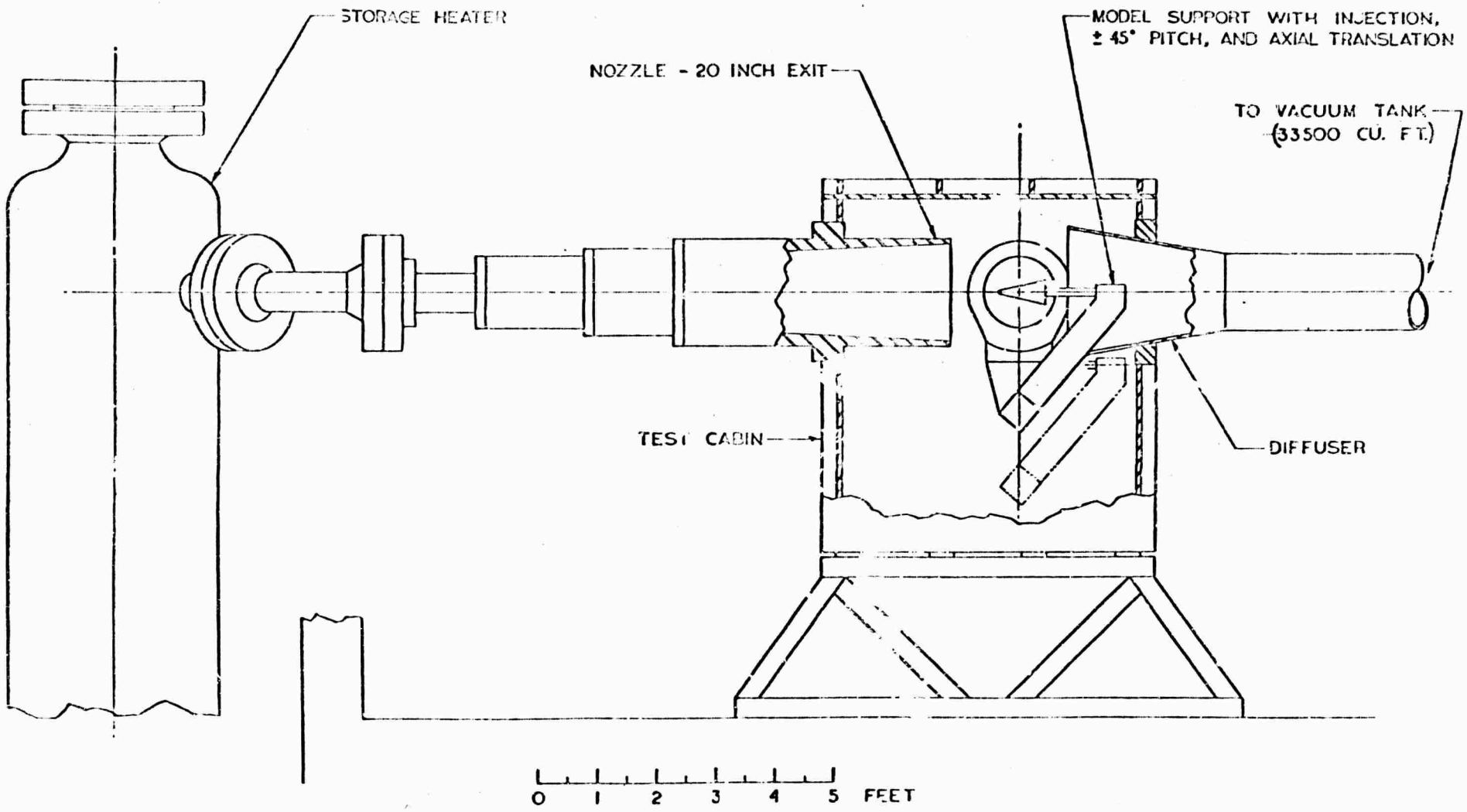


FIG. 1 THE 20-IN. HYPERSONIC TUNNEL

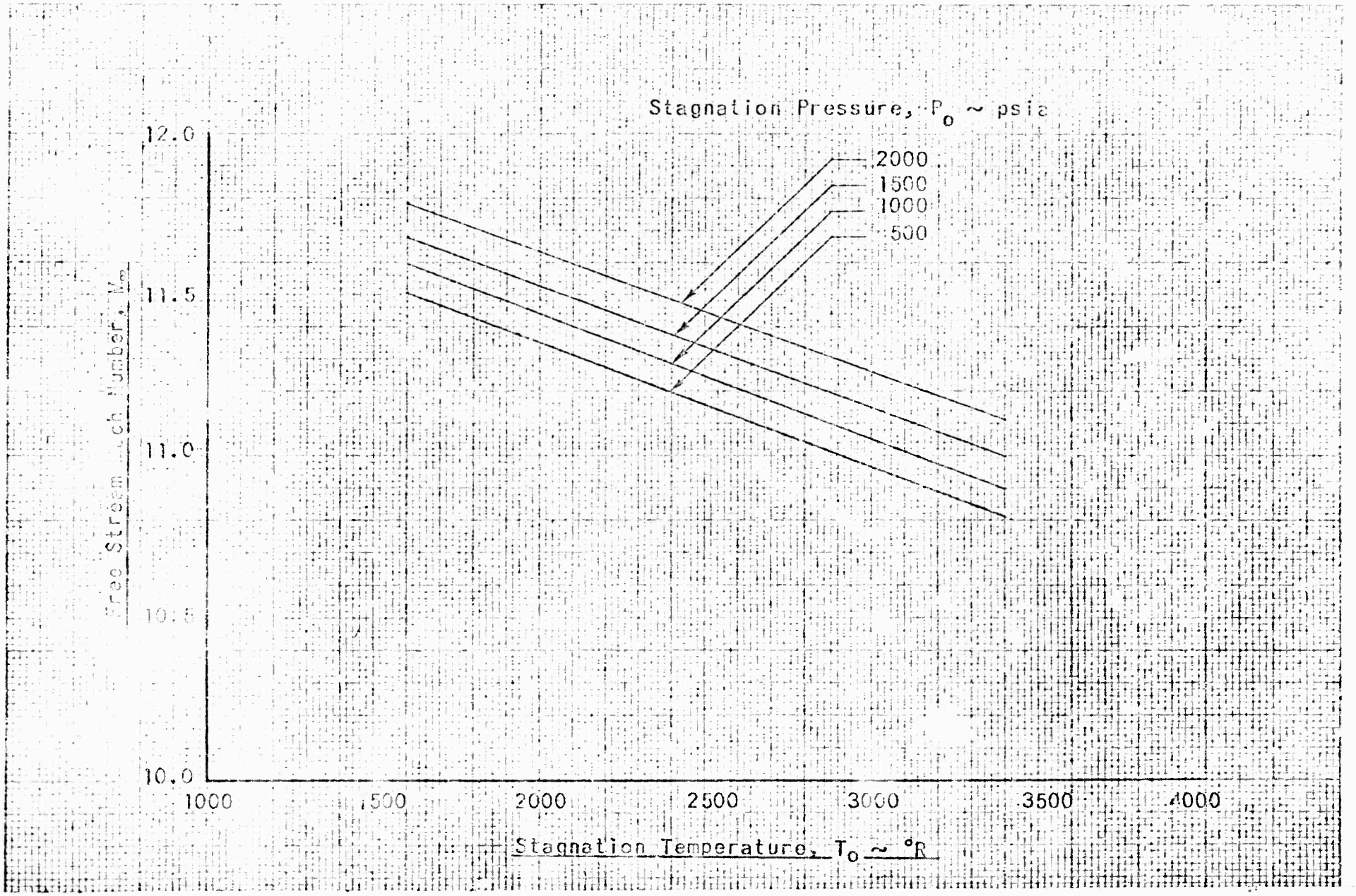


FIGURE 2 VARIATION IN TEST SECTION MACH NUMBER WITH $P_o$ AND $T_o$ FOR THE MACH 11.5 NOZZLE

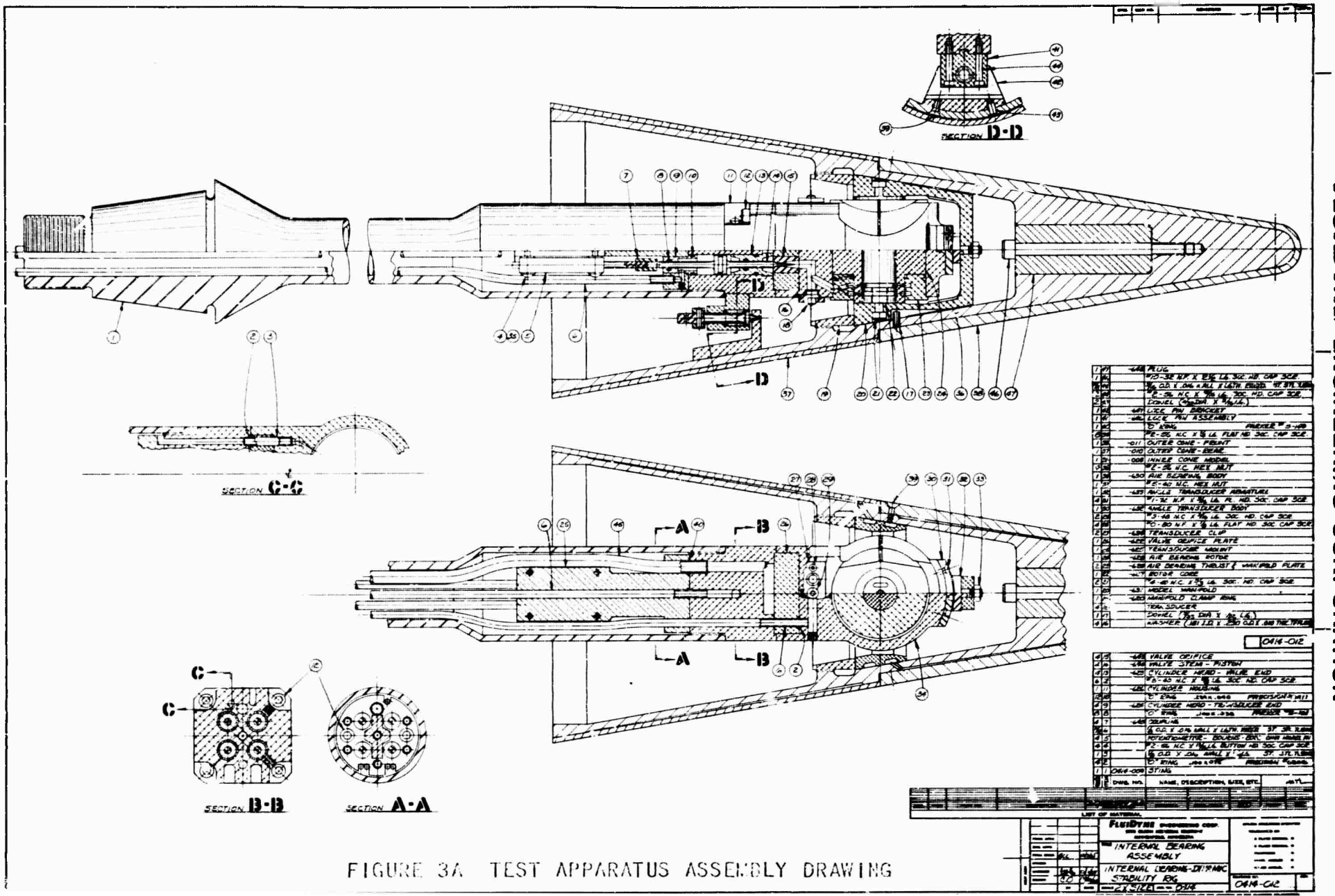


FIGURE 3A TEST APPARATUS ASSEMBLY DRAWING

FLUIDYNE ENGINEERING CORPORATION

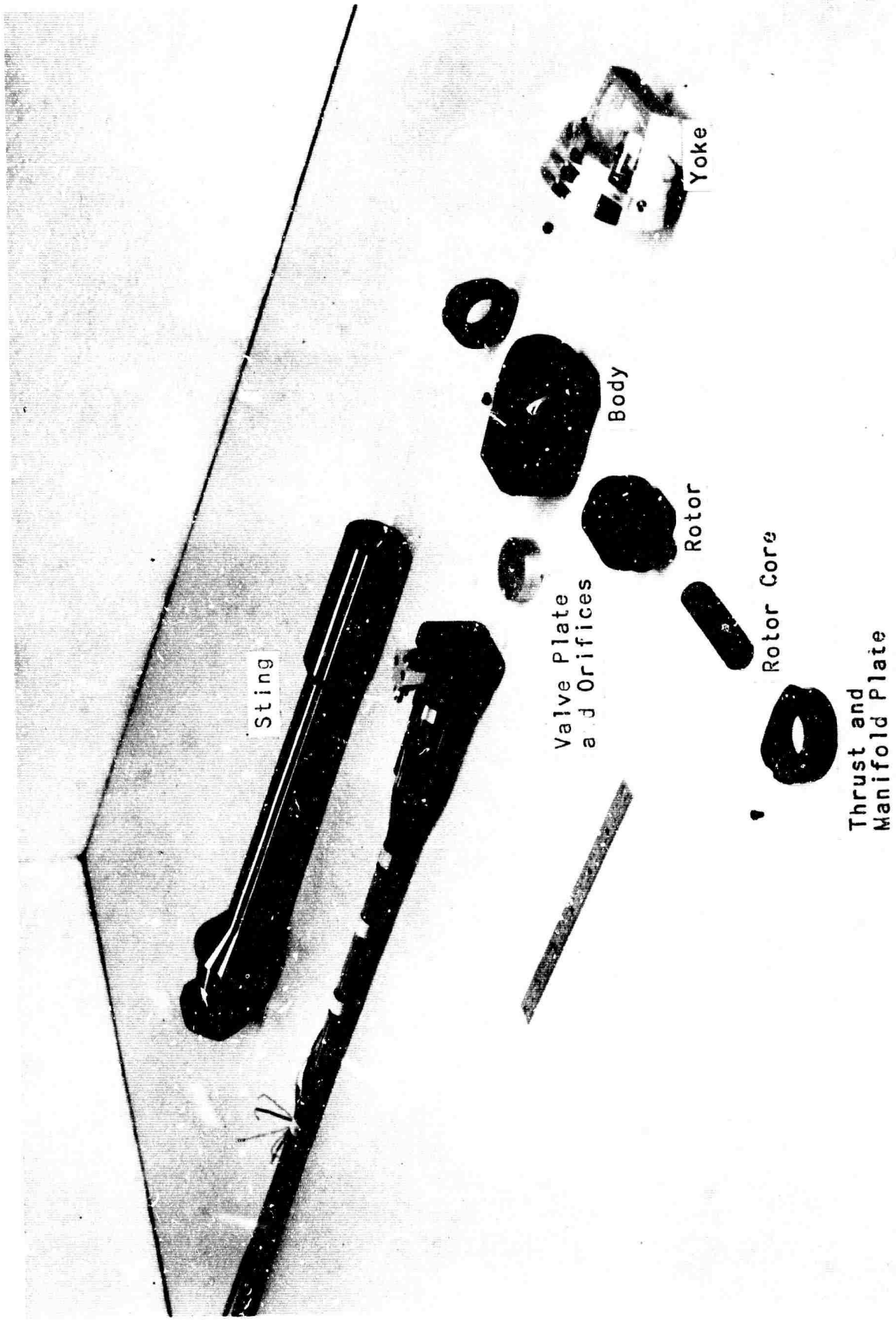


FIGURE 3B TEST APPARATUS DETAILS

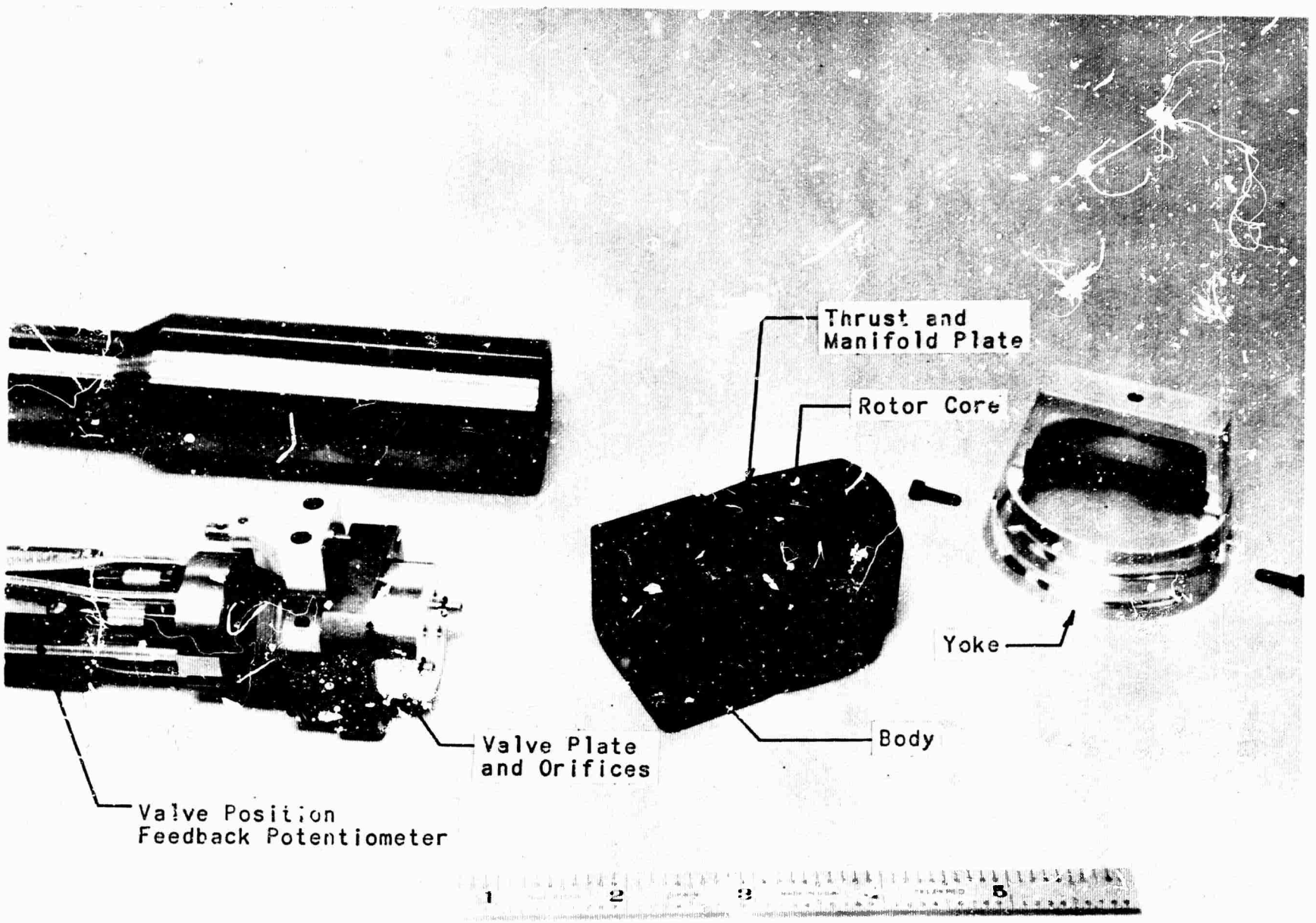
Thrust and
Manifold Plate
Rotor Core
Yoke
Body
Valve Plate
and Orifices
Valve Position
Feedback Potentiometer

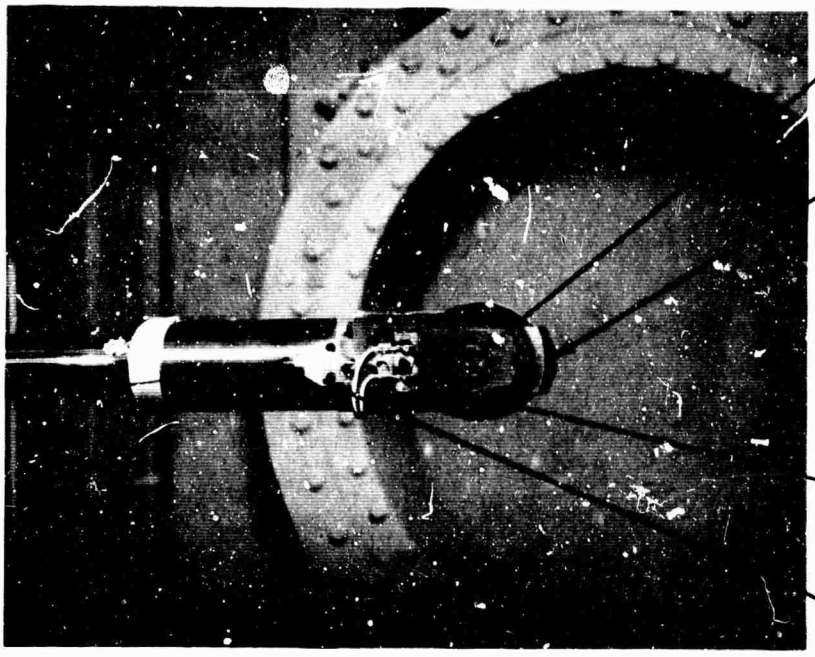



FIGURE 4 STING MOUNTED AIR BEARING

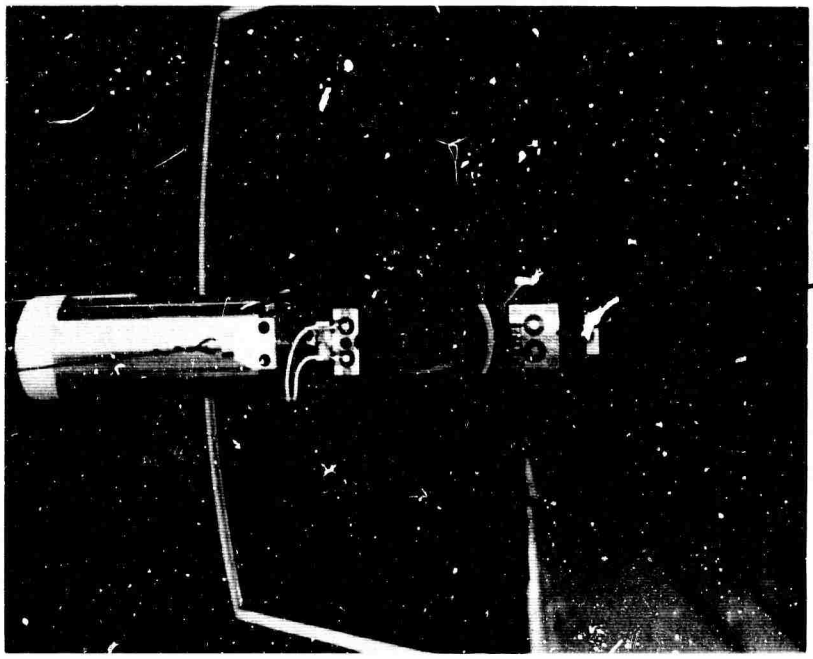


STING MOUNTED AIR BEARING

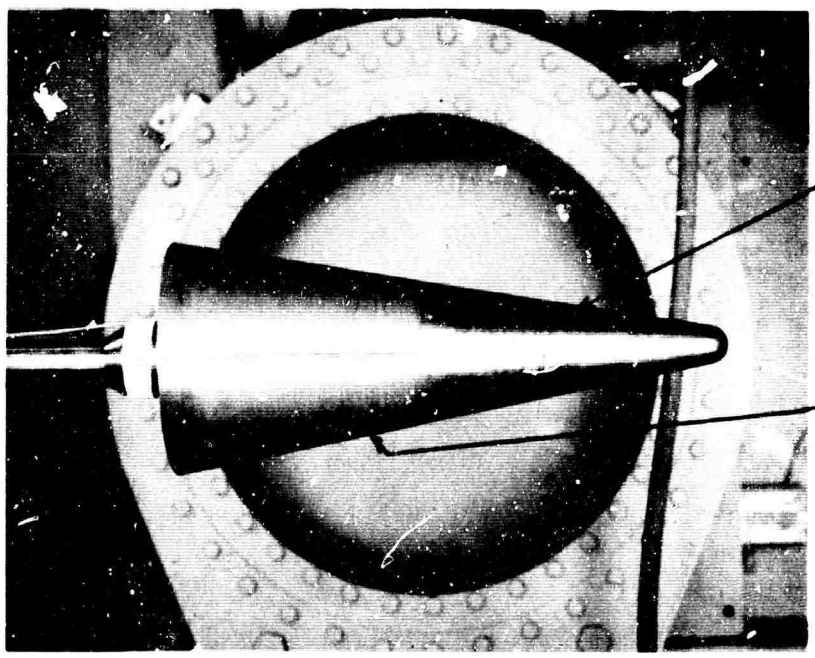


POROUS MODEL MOUNTED ON BEARING

FIGURE 5 TEST APPARATUS INSTALLED IN WIND TUNNEL

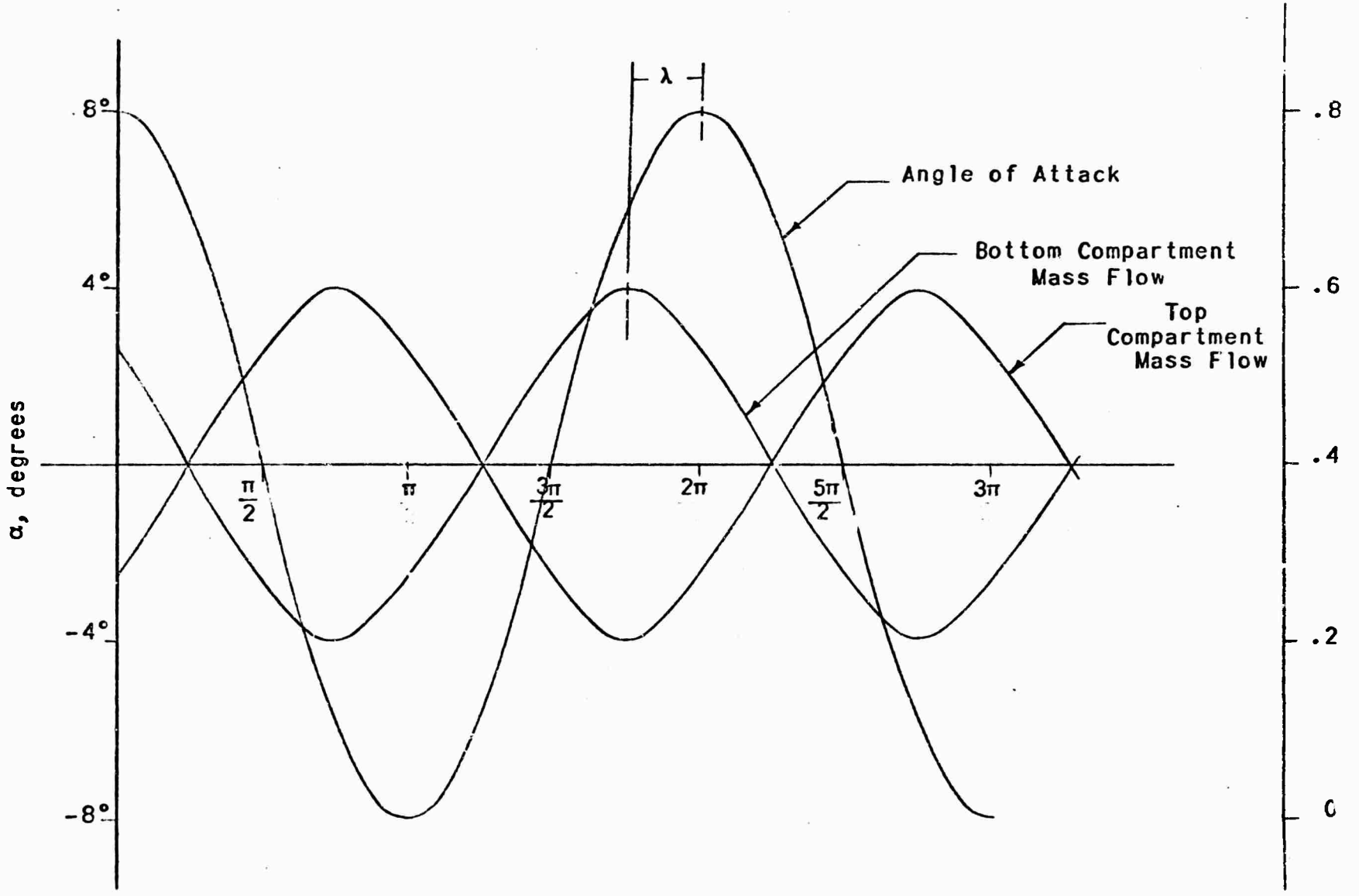


FIGURE 6 MASS FLOW - ANGLE OF ATTACK RELATIONSHIPS

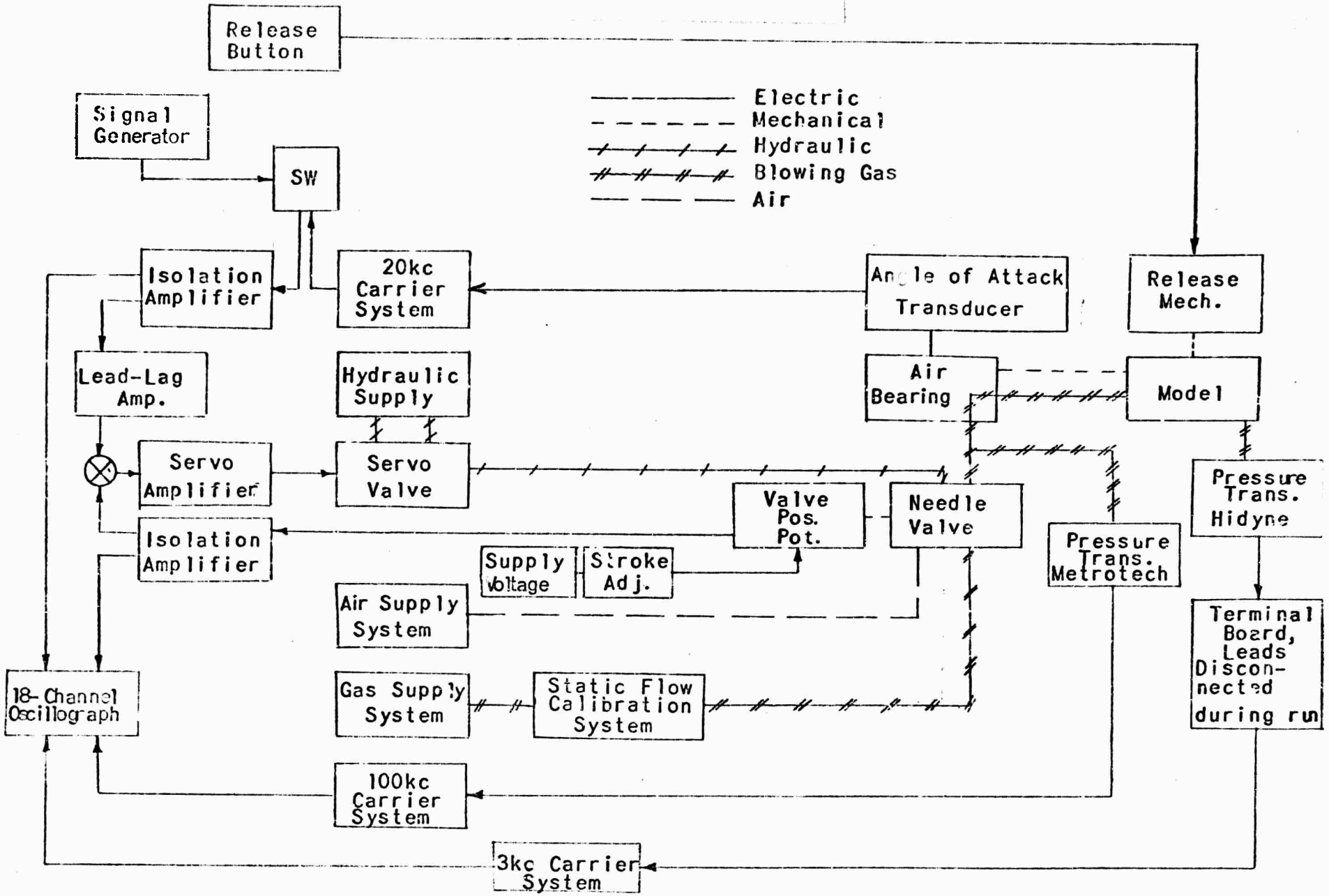


FIGURE 7 MASS TRANSFER SYSTEM - BLOCK DIAGRAM

FLUIDYNE ENGINEERING CORPORATION

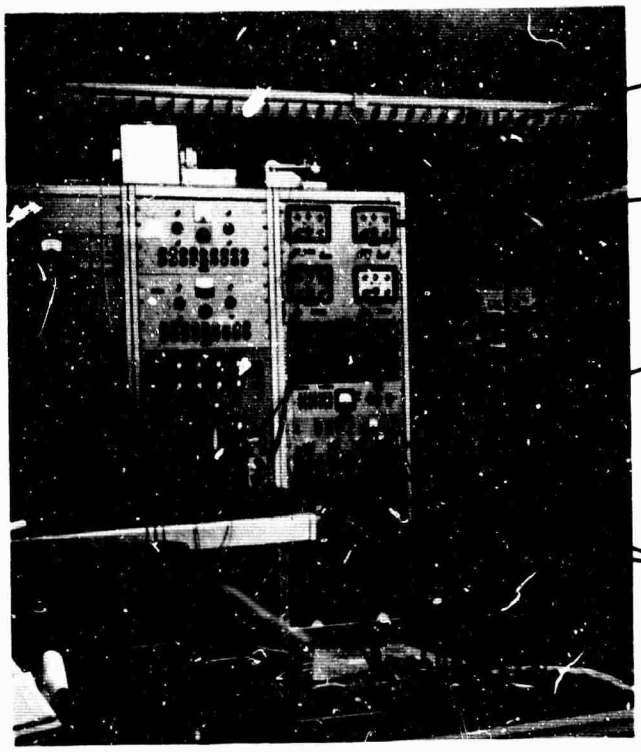

Signal Generator - Model Oscillation Simulator

100kc Carrier Amplifier for Metrotech Pressure Transducers, 4 Units

Valve Position Feedback Potentiometer Power Supply, Valve Bias Control Unit and 20kc Angle of Attack Carrier Amplifier

Operational Amplifiers

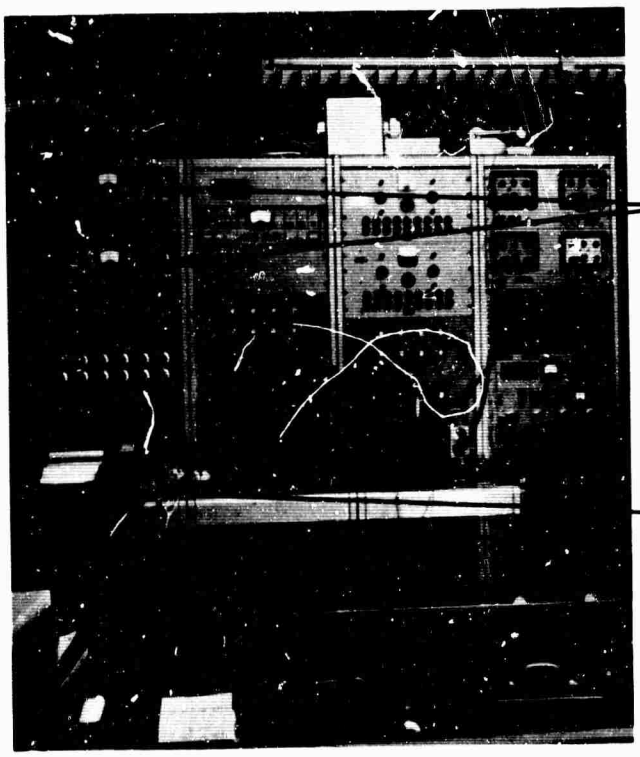

3kc Carrier Amplifiers for Hidyne Pressure Transducers

18 Channel Oscillograph

FIGURE 8 MASS FLOW CONTROL - CONSOLE INSTALLED COMPONENTS

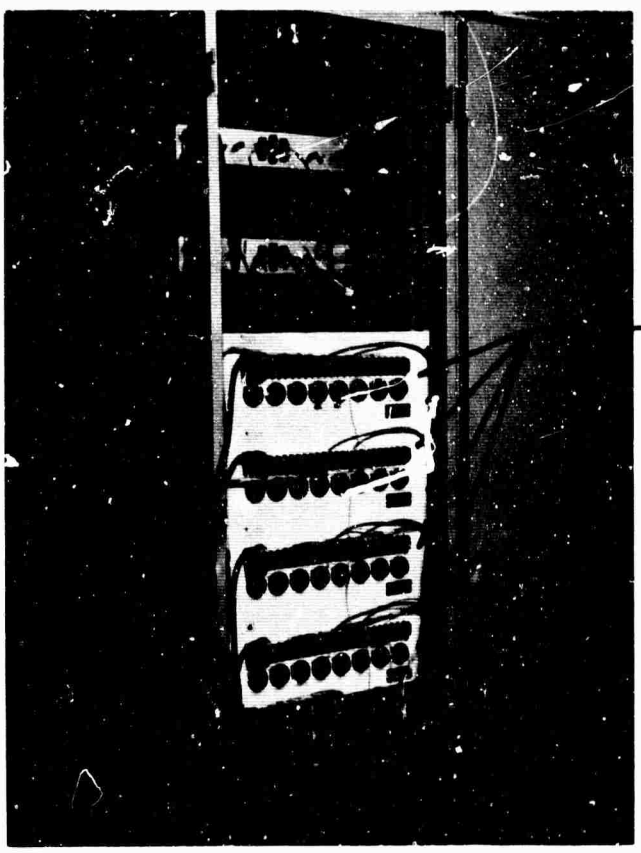


FIGURE 9 MASS FLOW CONTROL - REAR VIEW OF CONTROL CONSOLE

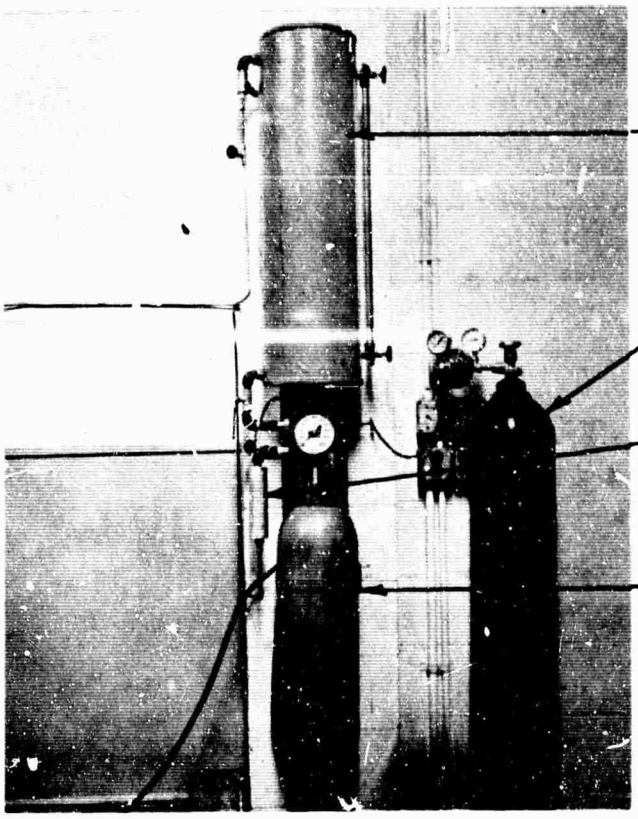


HYDRAULIC POWER SUPPLY

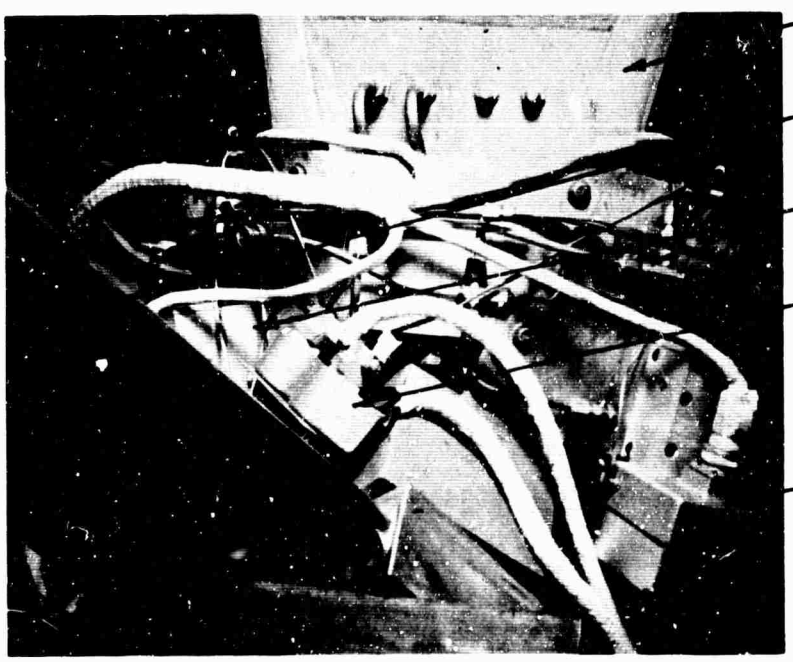


STRUT MOUNTED SERVO VALVES

FIGURE 10 MASS FLOW CONTROL - HYDRAULIC COMPONENTS

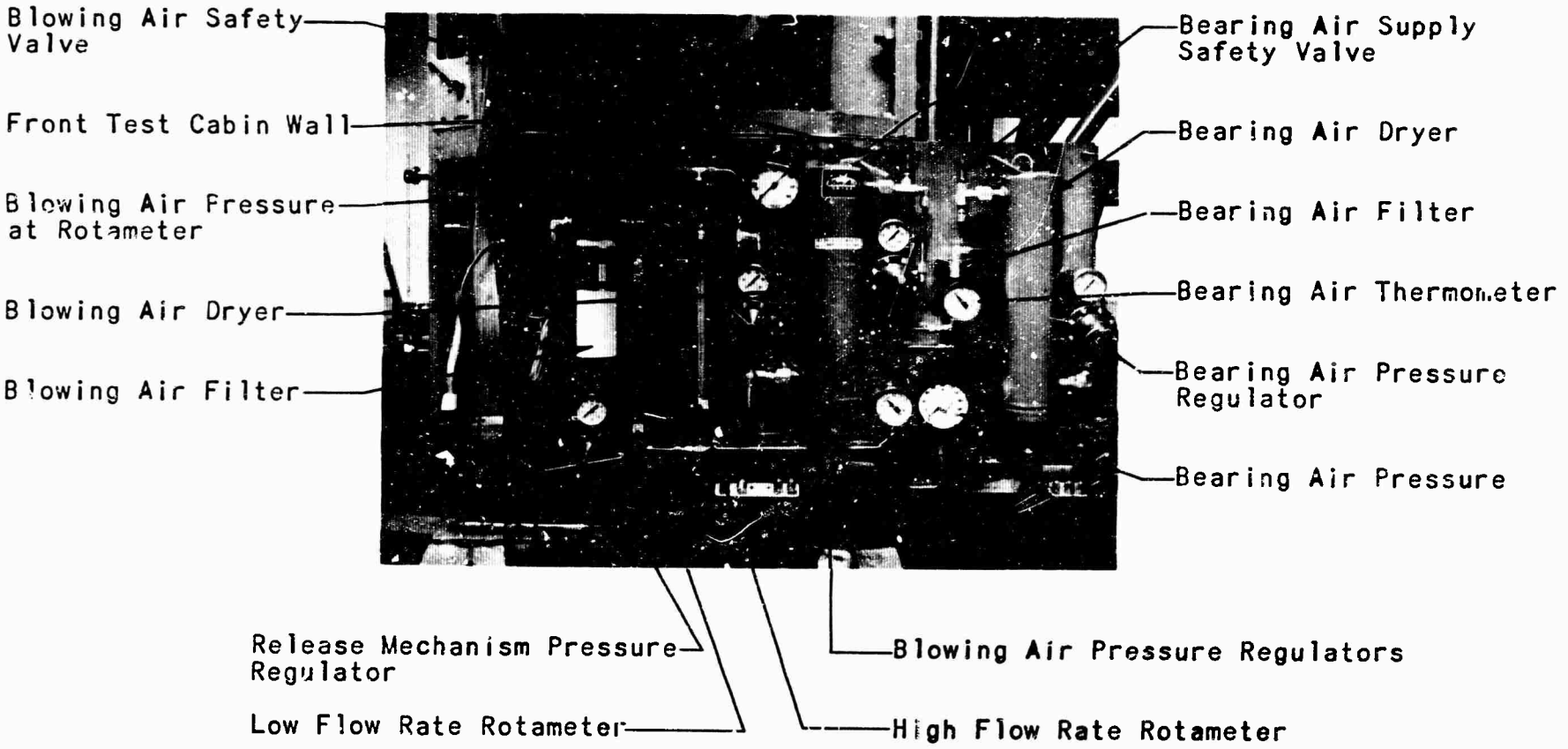


FIGURE 11 MASS FLOW CONTROL - PNEUMATIC CONTROL PANEL

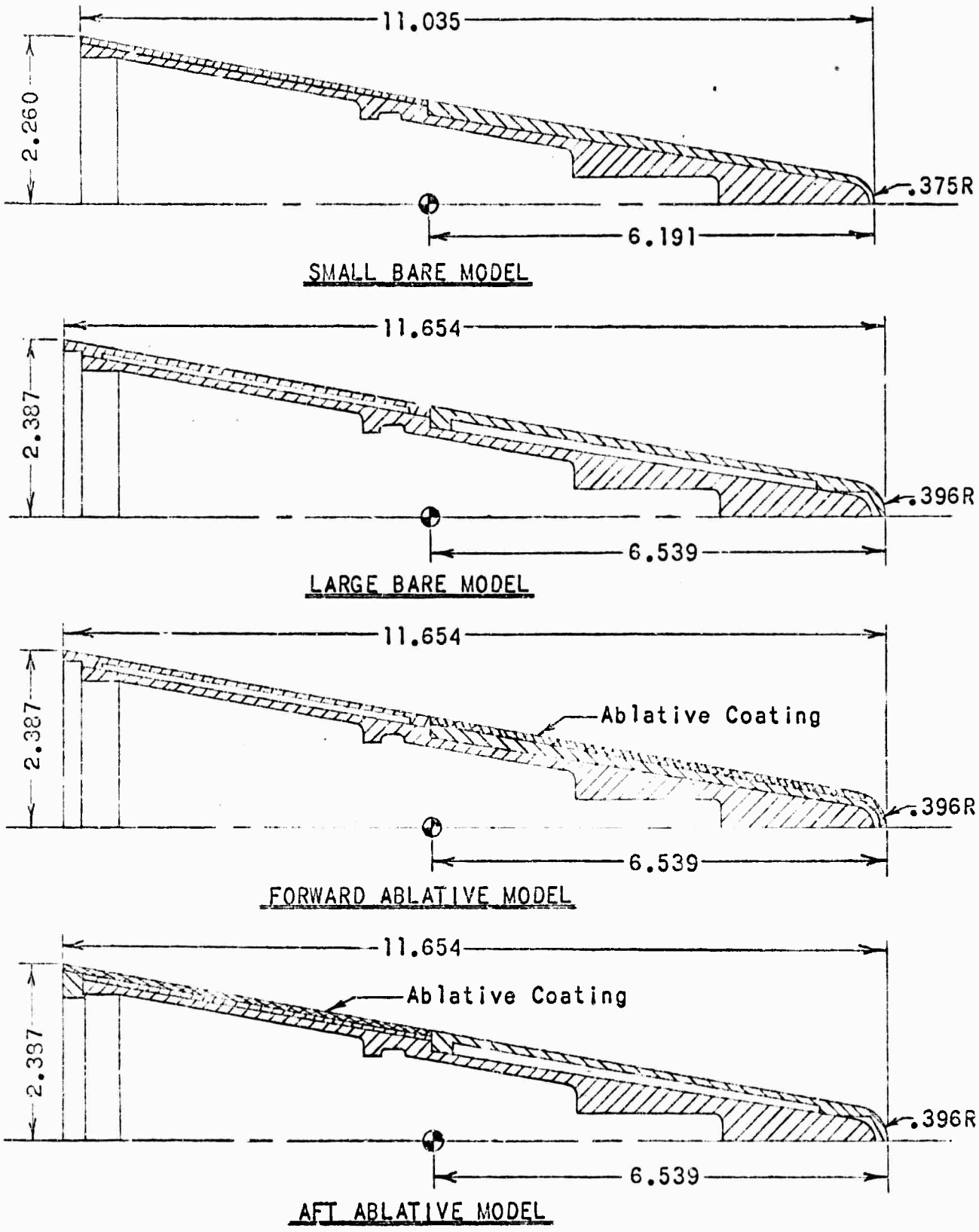


FIGURE 12 ABLATIVE MODEL DETAILS

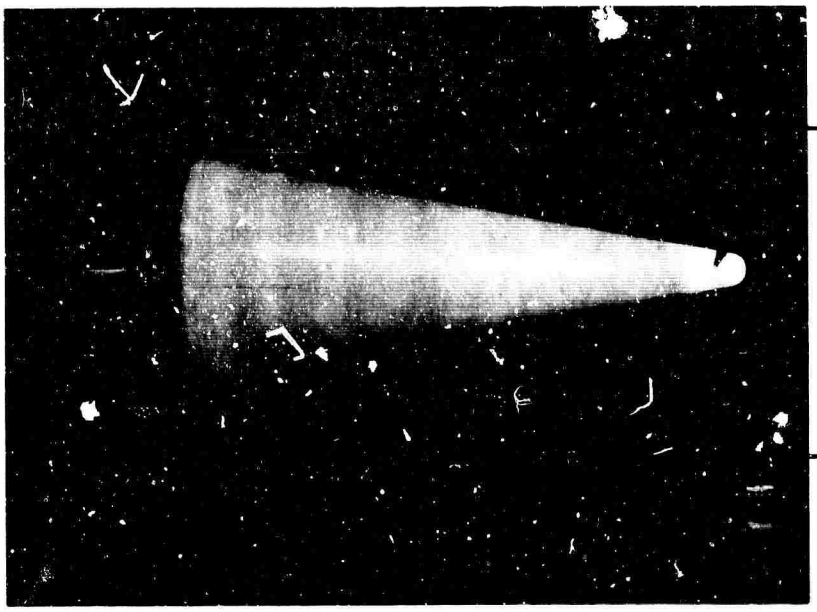


FULLY COATED

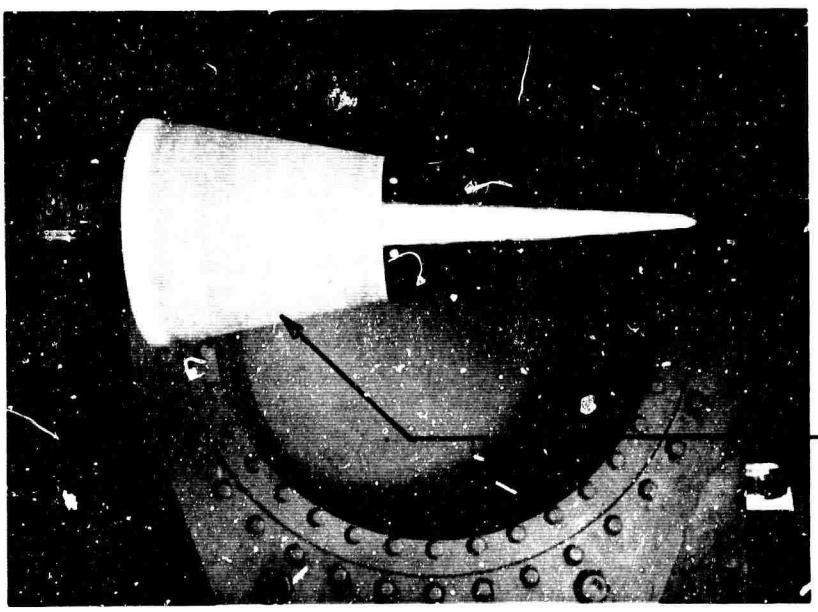


AFT SECTION COATED

FIGURE 13 ABLATIVE MODEL AFT AND FULLY COATED

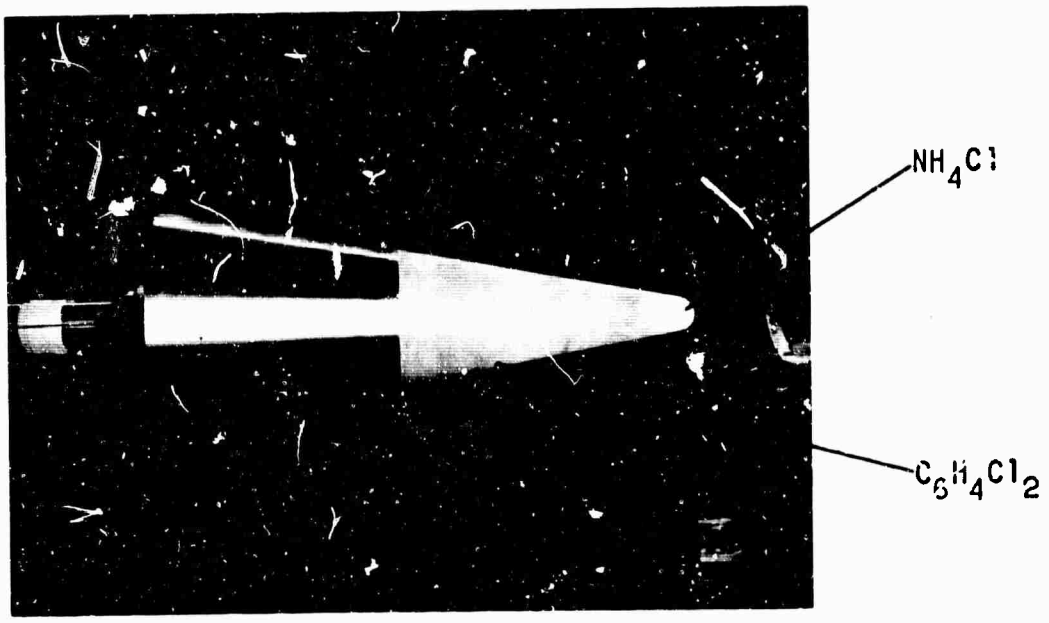


BEFORE RUN

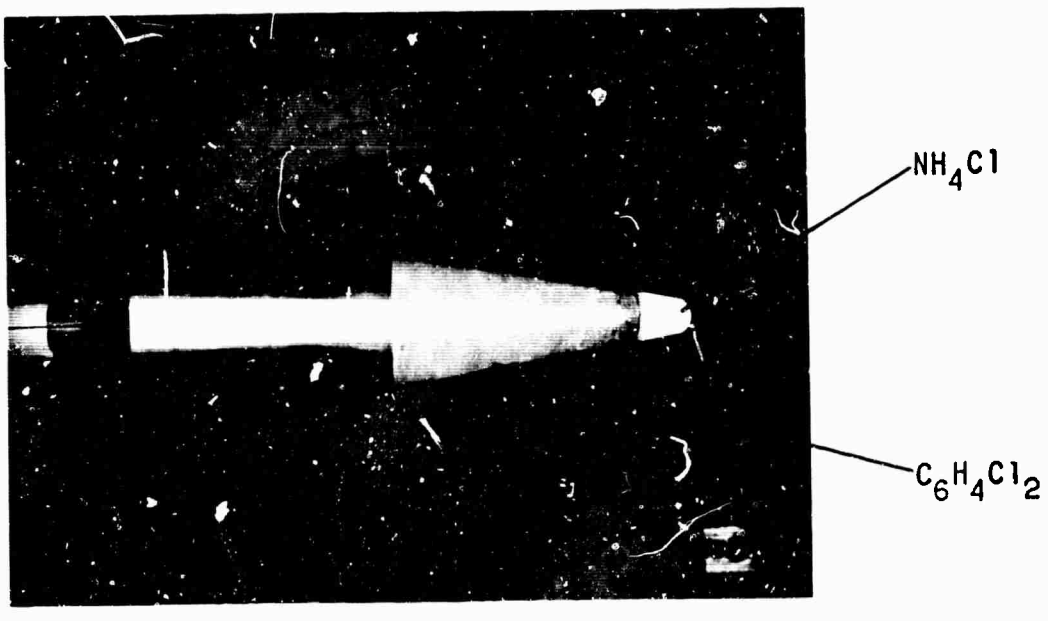


AFTER RUN

FIGURE 14 FORWARD ABLATIVE MODEL - TEST EFFECTS

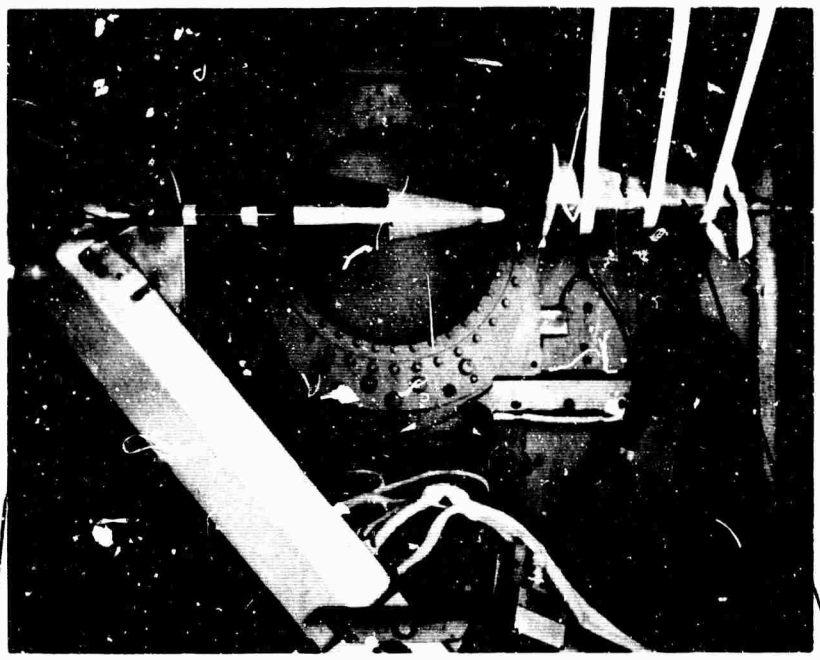


FIGURE 15 ABLATIVE MODEL IN TEST CABIN

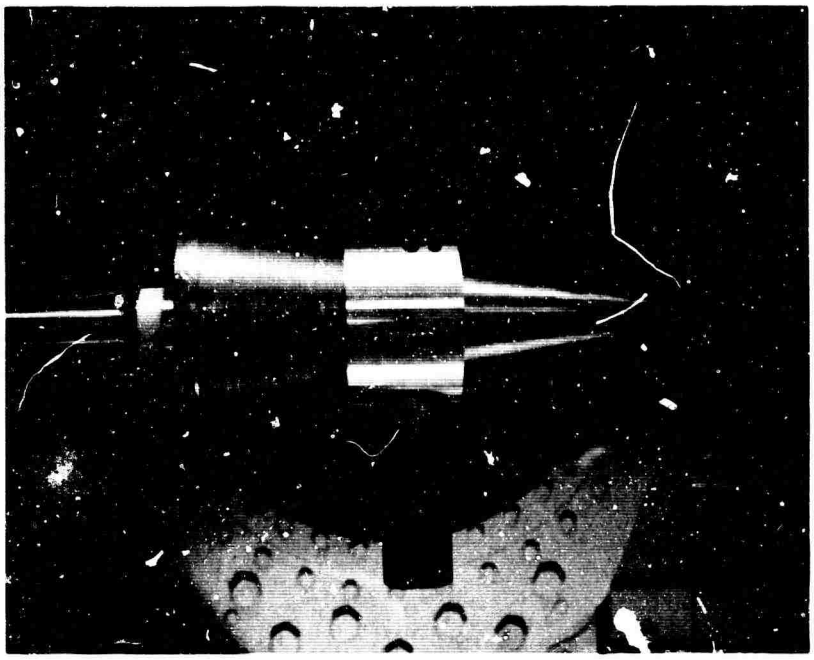

MODEL AND PENDULUM MOUNTED ON AIR BEARING

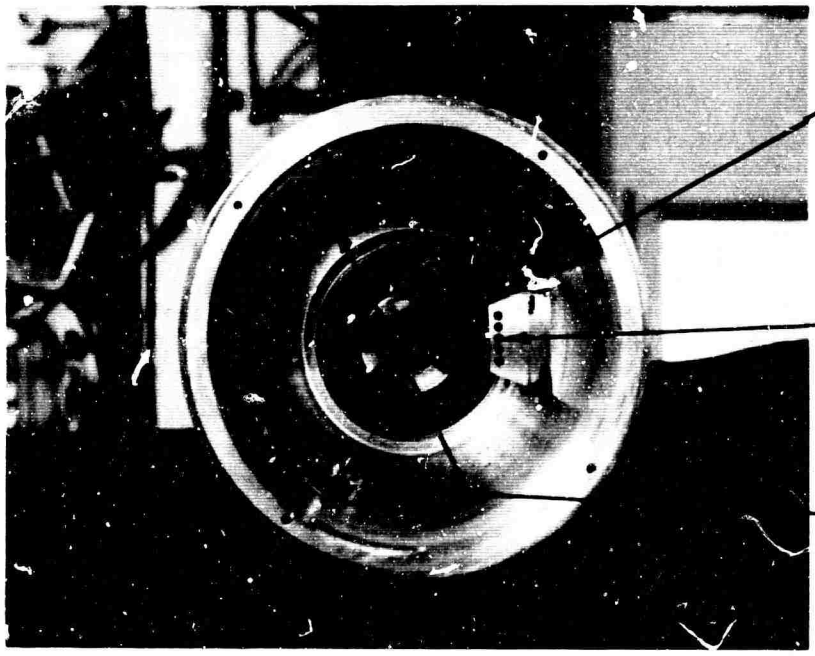


BASE VIEW OF MODEL

FIGURE 16 MODEL DAMPING CALIBRATION SETUP AND INTERNAL HARDWARE

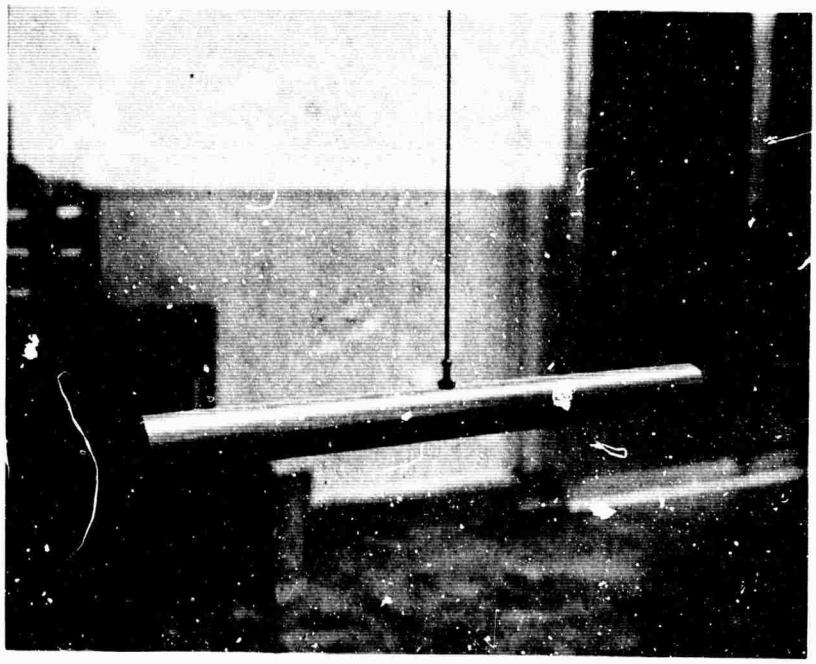

STANDARD BAR ON TORSION PENDULUM

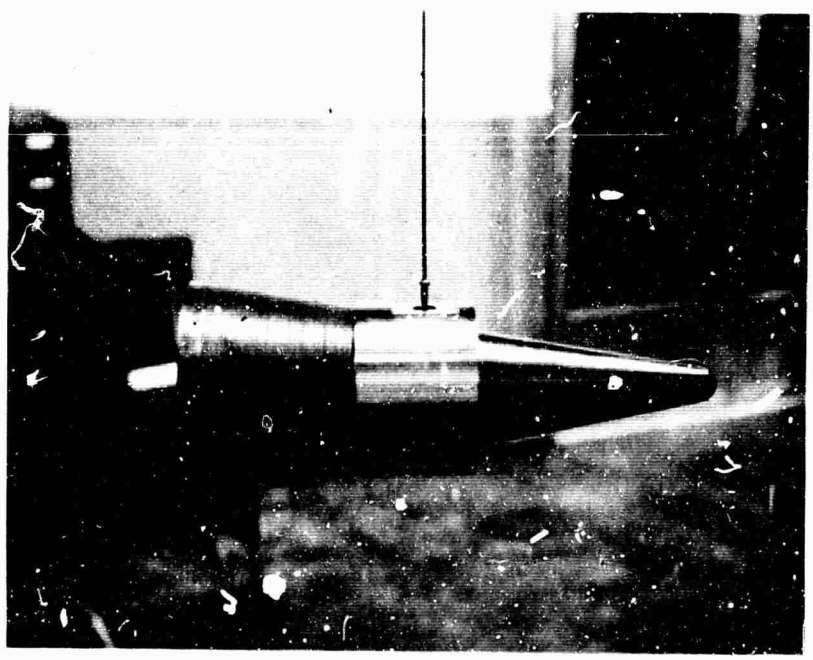

MODEL AND ADAPTOR ON TORSION PENDULUM

FIGURE 17 MOMENT OF INERTIA CALIBRATION SETUP

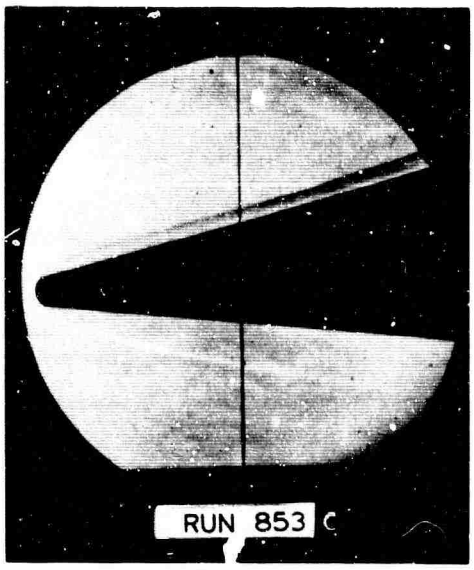


$\alpha = -4.2^{o}$ (Decreasing)


$\alpha = +3.8^{o}$ (Decreasing)

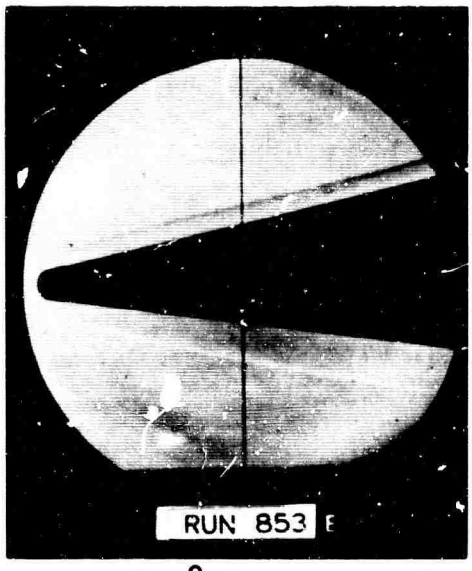


$\alpha = -1.9^{o}$ (Decreasing)


$\alpha = +0.1^{o}$ (Decreasing)

Run 853

$P_o = 995$ psia $\quad T_o = 2430^{o}R \quad M = 11.25$

FIGURE 18 SCHLIEREN PHOTOGRAPHS

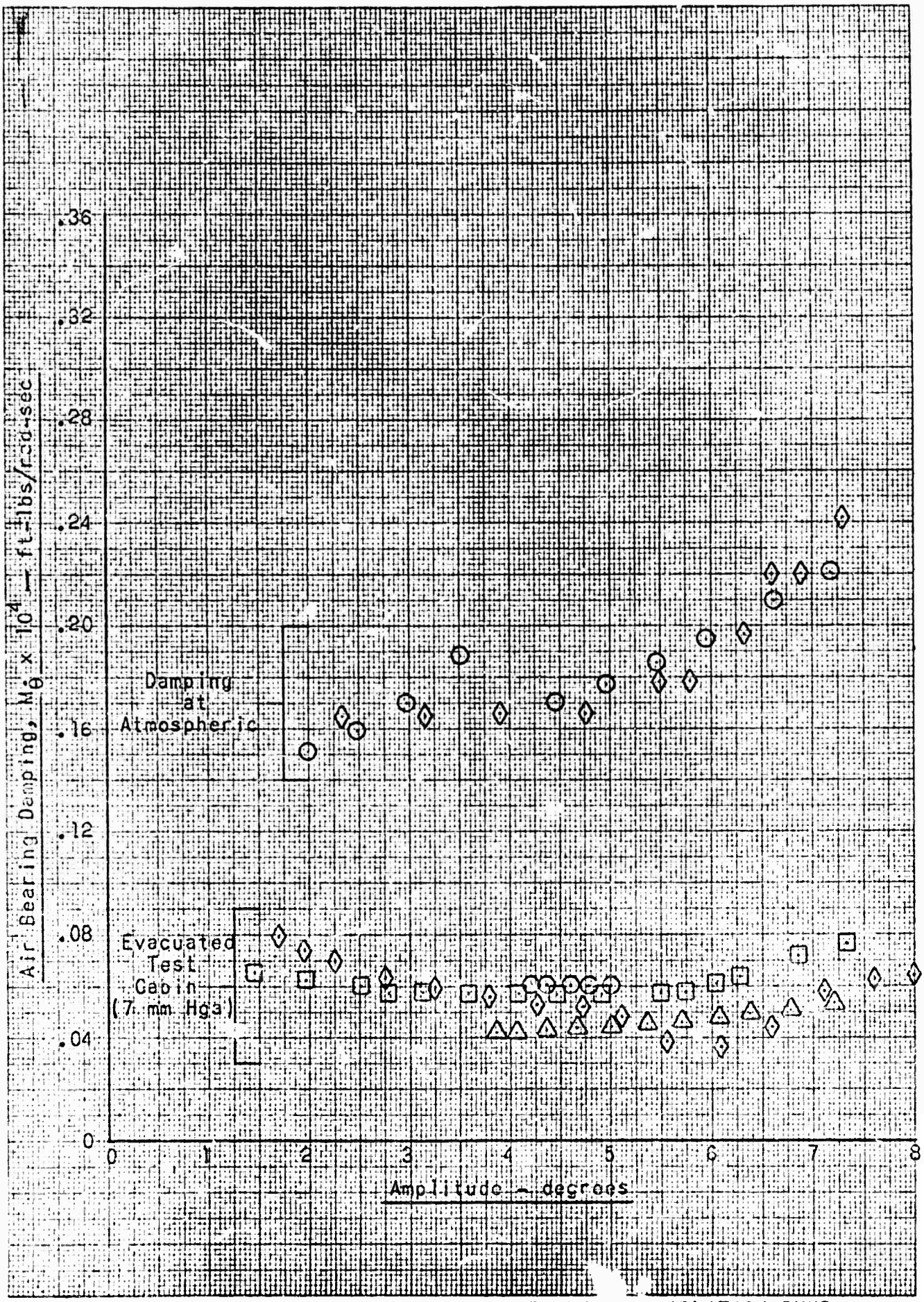


FIGURE 19 BEARING DAMPING CHARACTERISTICS - ABLATION RUNS

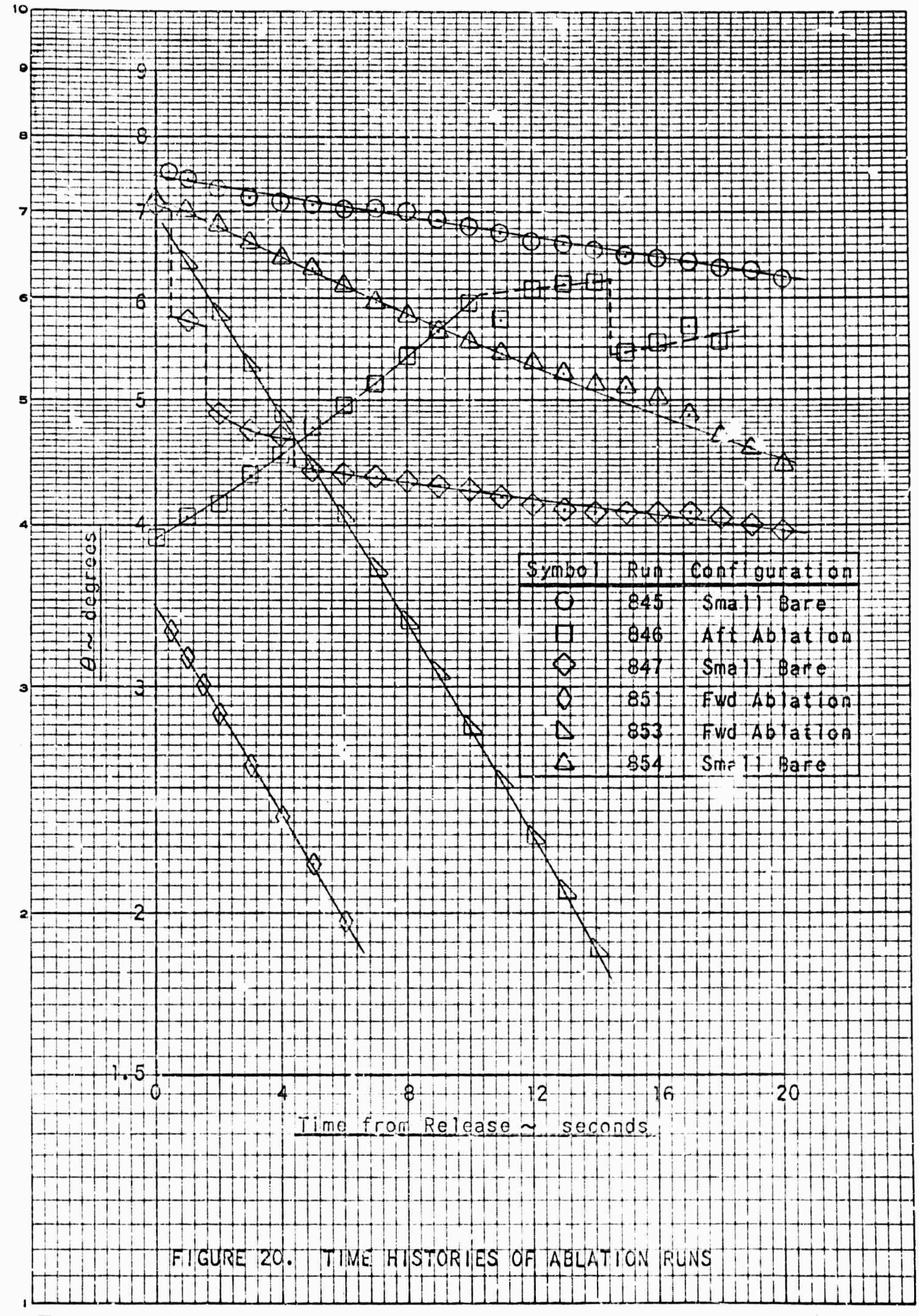


FIGURE 20. TIME HISTORIES OF ABLATION RUNS

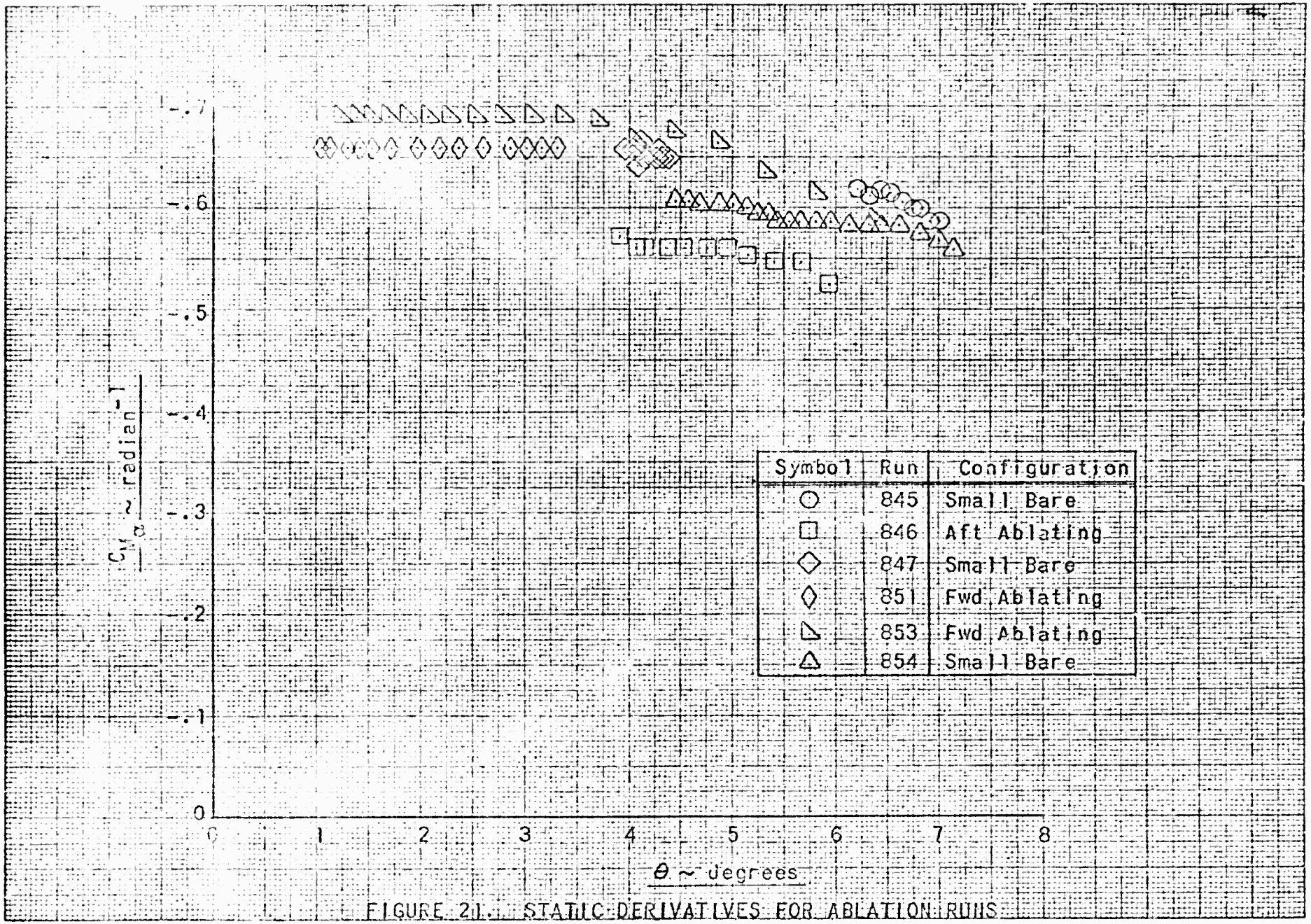


FIGURE 21. STATIC DERIVATIVES FOR ABLATION RUNS

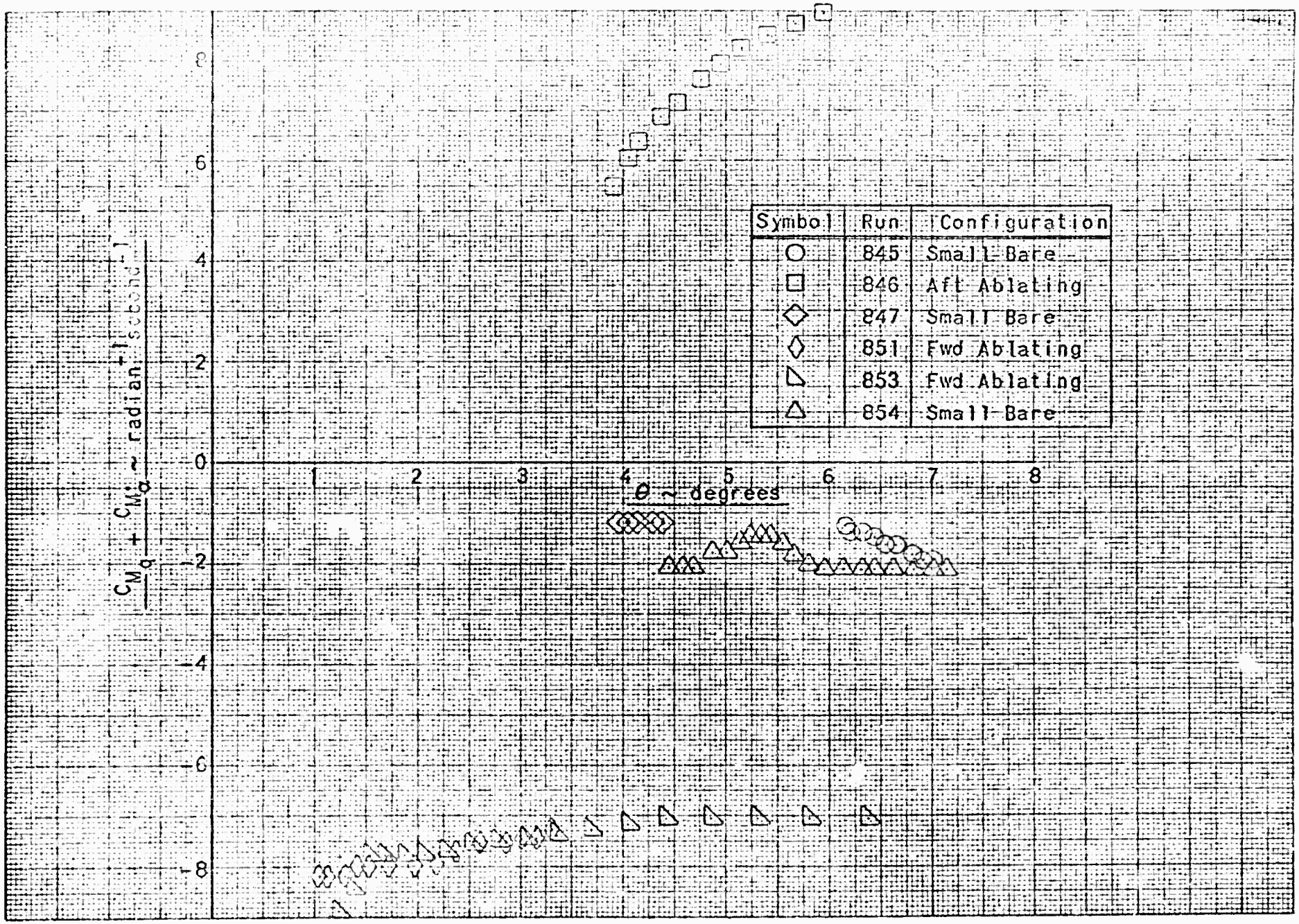


FIGURE 22. DYNAMIC DERIVATIVES FOR ABLATION RUNS

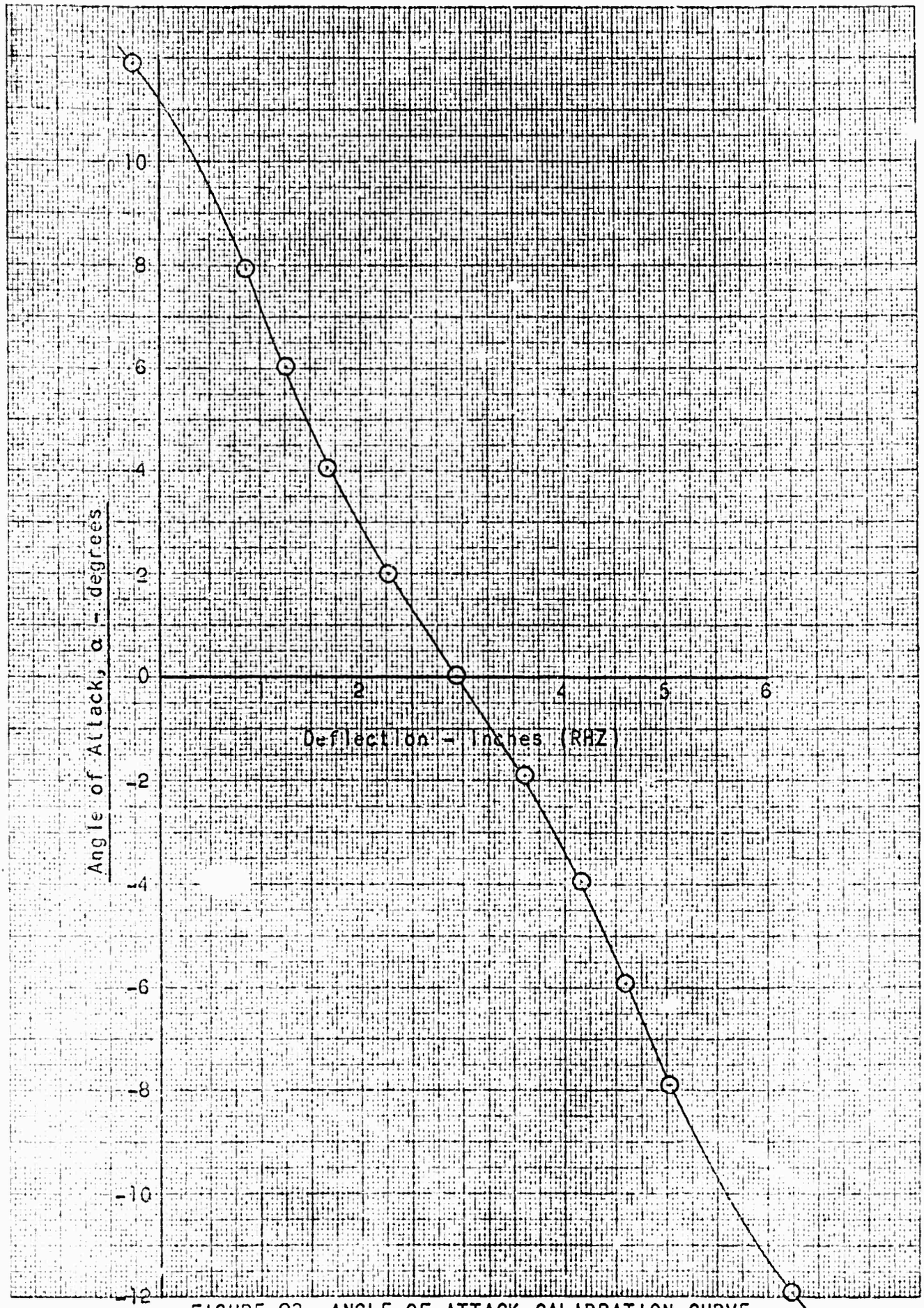


FIGURE 23 ANGLE OF ATTACK CALIBRATION CURVE

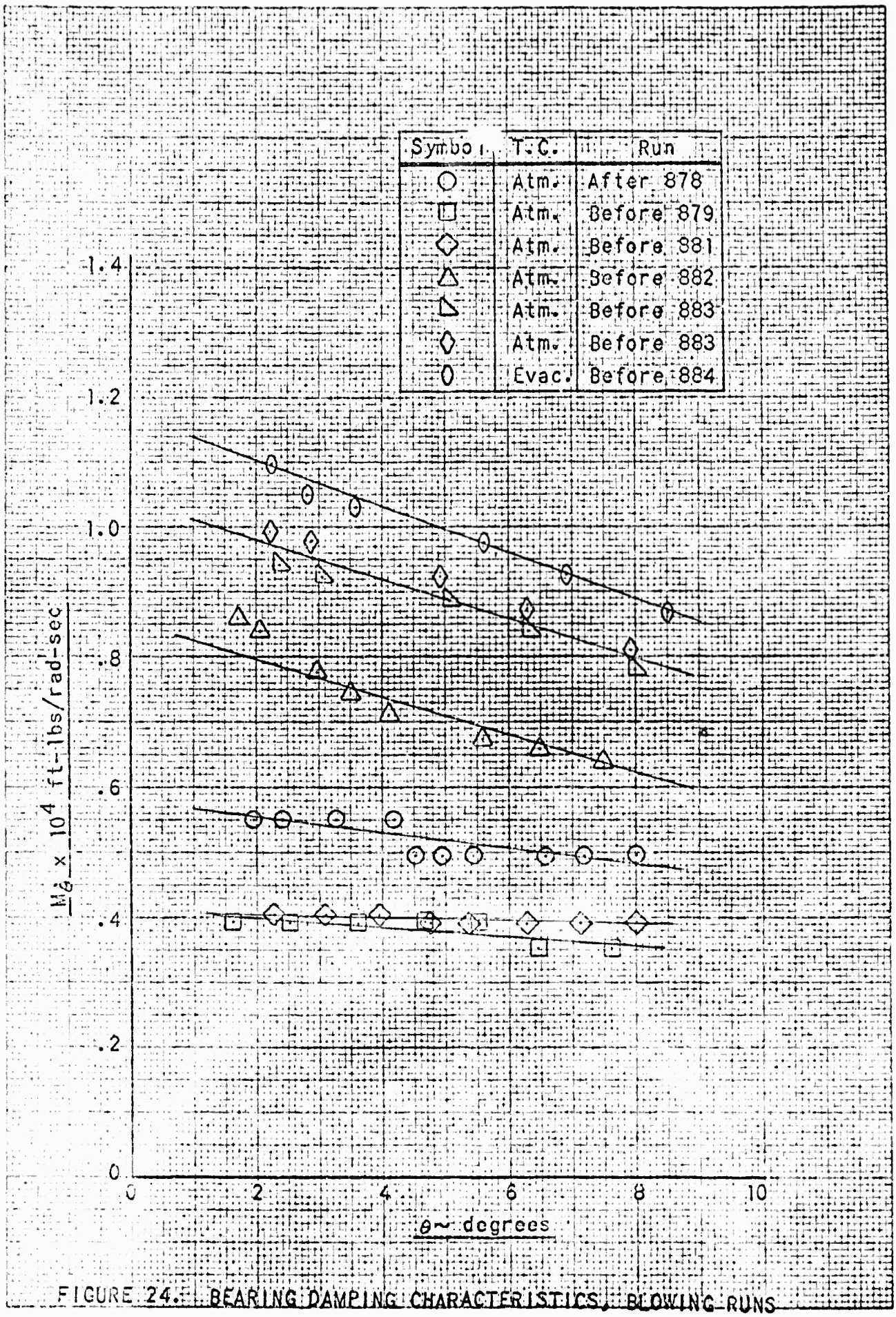


FIGURE 24. BEARING DAMPING CHARACTERISTICS, BLOWING RUNS

**FLUIDYNE ENGINEERING CORPORATION**

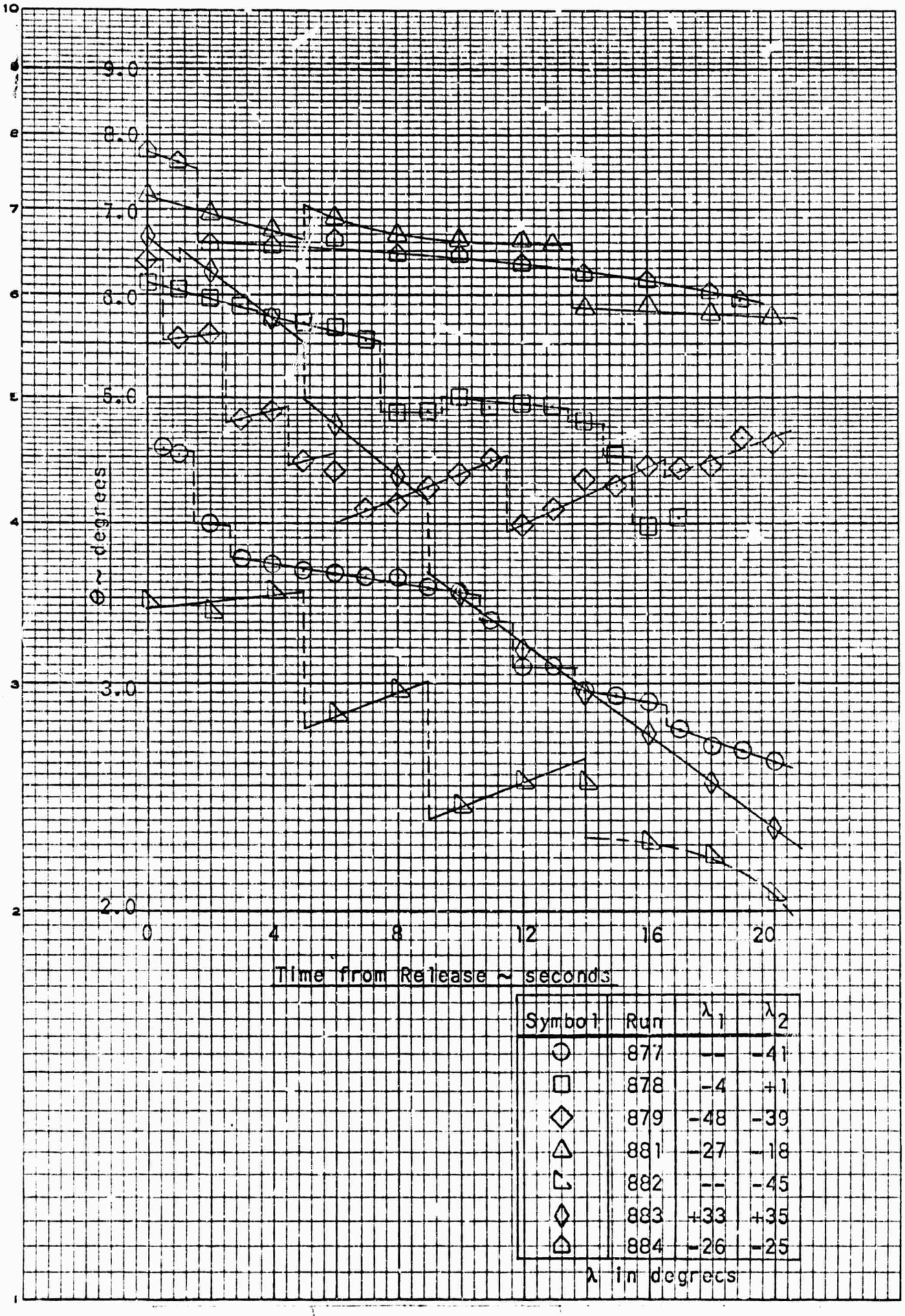


EUGENE DIETZGEN CO.
MADE IN U. S. A.

NO. 340R-L110 DIETZGEN GRAPH PAPER
SEMI-LOGARITHMIC
1 CYCLES X 10 DIVISIONS PER INCH

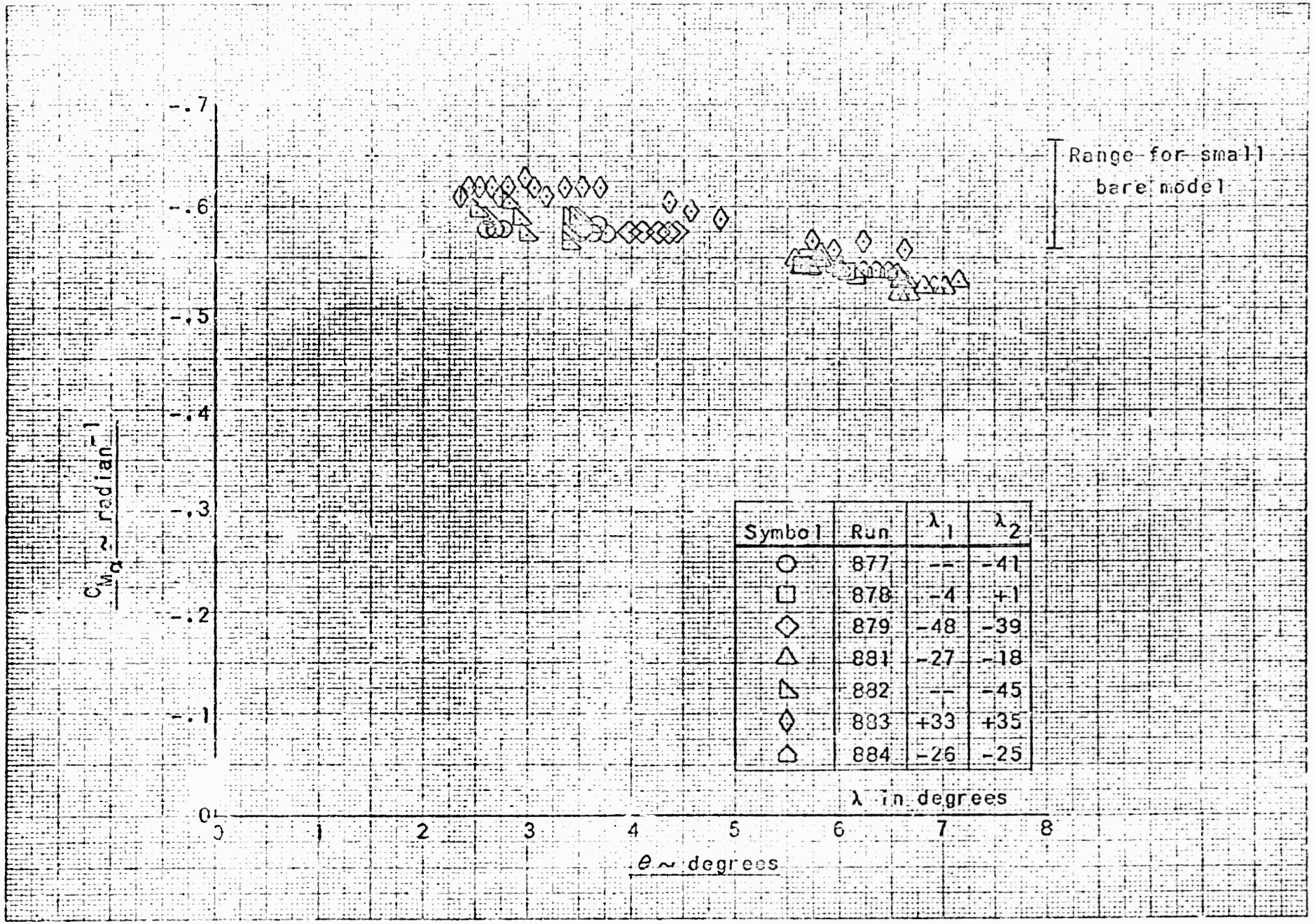


FIGURE 26. STATIC DERIVATIVES FOR BLOWING RUNS

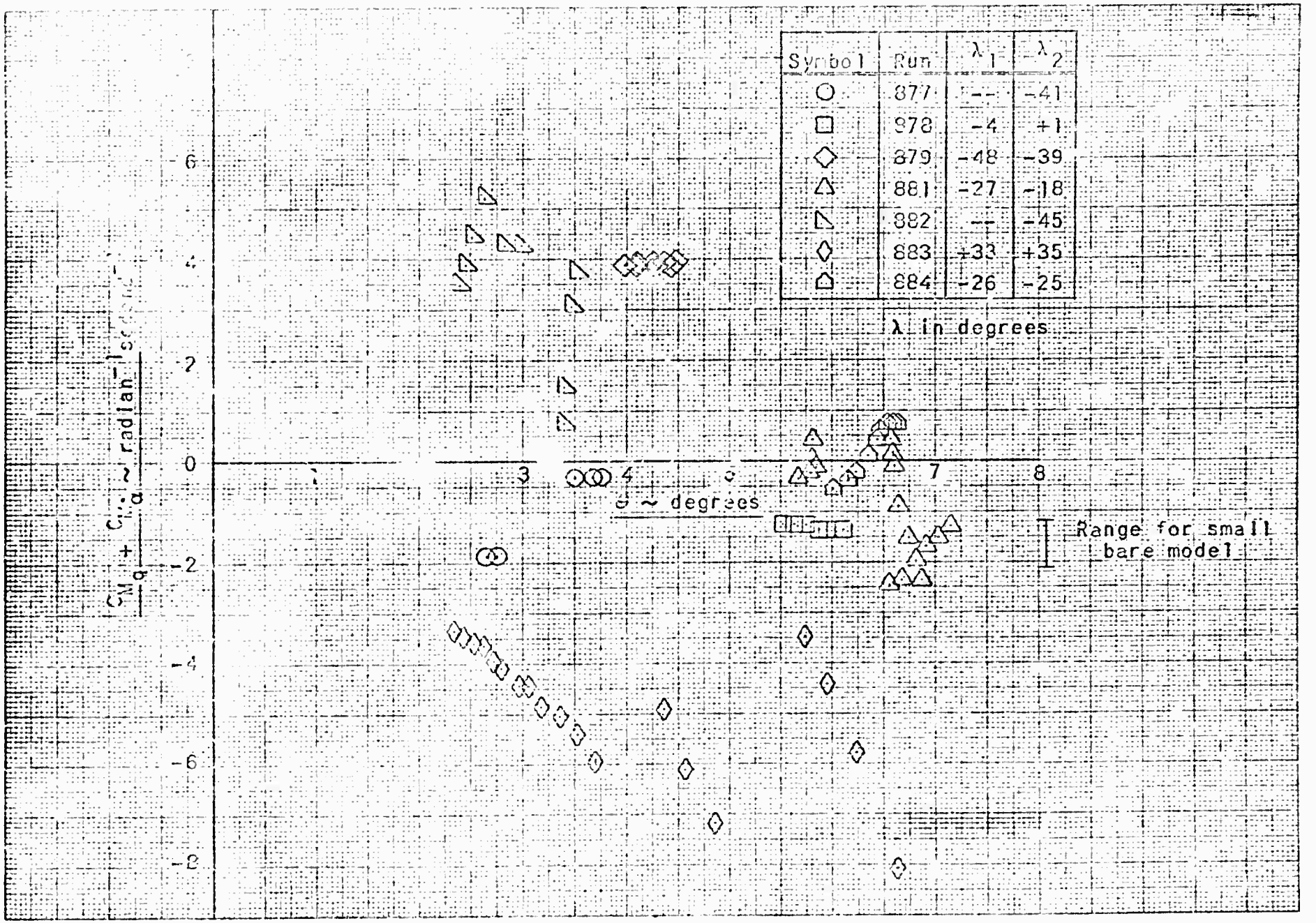


FIGURE 27. DYNAMIC DERIVATIVES FOR BLOWING RUNS

UNCLASSIFIED
Security Classification

**DOCUMENT CONTROL DATA - R&D**
*(Security classification of title, body of abstract and indexing annotation must be entered when the overall report is classified)*

1 ORIGINATING ACTIVITY (Corporate author)
FluiDyne Engineering Corporation

2a REPORT SECURITY CLASSIFICATION
UNCLASSIFIED

2b GROUP
N/A

3 REPORT TITLE
Wind Tunnel Tests Employing Temporal and Spatial Variations in Mass Transfer Distribution Through a Conical Surface to Control Aerodynamic Pitching Moment Characteristics.

4 DESCRIPTIVE NOTES (Type of report and inclusive dates)
Final technical report on a study on stability of re-entry vehicle models.

5 AUTHOR(S) (Last name, first name, initial)
Ibrahim, S. K.
Smith, K. W.
Pollock, R. B.
Christopherson, C. D.

| 6 REPORT DATE | 7a. TOTAL NO. OF PAGES | 7b. NO. OF REFS |
|---|---|---|
| 31 March 1967 | 91 | 6 |

| 8a CONTRACT OR GRANT NO. | 9a. ORIGINATOR'S REPORT NUMBER(S) |
|---|---|
| Nonr-4624(00) | 0414-3-31-67 |
| b. PROJECT NO. | |
| c. | 9b. OTHER REPORT NO(S) (Any other numbers that may be assigned this report) |
| d. | |

10. AVAILABILITY/LIMITATION NOTICES

| 11. SUPPLEMENTARY NOTES | 12. SPONSORING MILITARY ACTIVITY |
|---|---|
| | ARPA Order No. 576 |

13 ABSTRACT This report describes an experimental study of the effects of mass transfer on the stability of conical bodies. A unique apparatus was created which permits the support of a conical model in a hypersonic wind tunnel with small pitch damping due to the apparatus, and at the same time provides a means for blowing through four separate (aft, forward, top, bottom combinations) model surface areas. Independent servo controls were provided for the flow through each surface section such that the mass transfer through the model wall could be varied both spatially and temporally. This apparatus was installed in the FluiDyne Hypersonic Wind Tunnel and tests were run at a nominal Mach number of 11. Runs were made without mass transfer, with mass transfer produced by a subliming material, and with mass transfer produced by blowing through a porous surface. These tests provided additional confirmation that mass transfer from a surface will, in itself, significantly influence the pitch damping characteristics of a conical shape whether its origin is in a heat transfer related phenomenon (such as ablation or sublimation) or an independently controlled flow process such as is represented by blowing through the conical surface. In addition, these tests provided an opportunity for shakedown of the blowing flow control apparatus; however, it was not possible to carry the blowing study into the parametric investigation initially planned within the present program. Thus, the interrelation of such parameters as mass flow, volume flow, spatial distribution, temporal distribution, etc., remain to be investigated in detail.

DD FORM 1473

UNCLASSIFIED
Security Classification

| 14 KEY WORDS | LINK A ROLE | LINK A WT | LINK B ROLE | LINK B WT | LINK C ROLE | LINK C WT |
|---|---|---|---|---|---|---|
| Re-entry | | | | | | |
| Dynamic Stability | | | | | | |
| Stability | | | | | | |
| Hypersonic | | | | | | |
| Mass Transfer | | | | | | |
| Damping Coefficients | | | | | | |

## INSTRUCTIONS

1. ORIGINATING ACTIVITY: Enter the name and address of the contractor, subcontractor, grantee, Department of Defense activity or other organization *(corporate author)* issuing the report.

2a. REPORT SECURITY CLASSIFICATION: Enter the overall security classification of the report. Indicate whether "Restricted Data" is included. Marking is to be in accordance with appropriate security regulations.

2b. GROUP: Automatic downgrading is specified in DoD Directive 5200.10 and Armed Forces Industrial Manual. Enter the group number. Also, when applicable, show that optional markings have been used for Group 3 and Group 4 as authorized.

3. REPORT TITLE: Enter the complete report title in all capital letters. Titles in all cases should be unclassified. If a meaningful title cannot be selected without classification, show title classification in all capitals in parenthesis immediately following the title.

4. DESCRIPTIVE NOTES: If appropriate, enter the type of report, e.g., interim, progress, summary, annual, or final. Give the inclusive dates when a specific reporting period is covered.

5. AUTHOR(S): Enter the name(s) of author(s) as shown on or in the report. Enter last name, first name, middle initial. If military, show rank and branch of service. The name of the principal author is an absolute minimum requirement.

6. REPORT DATE: Enter the date of the report as day, month, year; or month, year. If more than one date appears on the report, use date of publication.

7a. TOTAL NUMBER OF PAGES: The total page count should follow normal pagination procedures, i.e., enter the number of pages containing information.

7b. NUMBER OF REFERENCES: Enter the total number of references cited in the report.

8a. CONTRACT OR GRANT NUMBER: If appropriate, enter the applicable number of the contract or grant under which the report was written.

8b, 8c, & 8d. PROJECT NUMBER: Enter the appropriate military department identification, such as project number, subproject number, system numbers, task number, etc.

9a. ORIGINATOR'S REPORT NUMBER(S): Enter the official report number by which the document will be identified and controlled by the originating activity. This number must be unique to this report.

9b. OTHER REPORT NUMBER(S): If the report has been assigned any other report numbers *(either by the originator or by the sponsor)*, also enter this number(s).

10. AVAILABILITY/LIMITATION NOTICES: Enter any limitations on further dissemination of the report, other than those imposed by security classification, using standard statements such as:

(1) "Qualified requesters may obtain copies of this report from DDC."

(2) "Foreign announcement and dissemination of this report by DDC is not authorized."

(3) "U. S. Government agencies may obtain copies of this report directly from DDC. Other qualified DDC users shall request through _____."

(4) "U. S. military agencies may obtain copies of this report directly from DDC. Other qualified users shall request through _____."

(5) "All distribution of this report is controlled. Qualified DDC users shall request through _____."

If the report has been furnished to the Office of Technical Services, Department of Commerce, for sale to the public, indicate this fact and enter the price, if known.

11. SUPPLEMENTARY NOTES: Use for additional explanatory notes.

12. SPONSORING MILITARY ACTIVITY: Enter the name of the departmental project office or laboratory sponsoring *(paying for)* the research and development. Include address.

13. ABSTRACT: Enter an abstract giving a brief and factual summary of the document indicative of the report, even though it may also appear elsewhere in the body of the technical report. If additional space is required, a continuation sheet shall be attached.

It is highly desirable that the abstract of classified reports be unclassified. Each paragraph of the abstract shall end with an indication of the military security classification of the information in the paragraph, represented as *(TS)*, *(S)*, *(C)*, or *(U)*.

There is no limitation on the length of the abstract. However, the suggested length is from 150 to 225 words.

14. KEY WORDS: Key words are technically meaningful terms or short phrases that characterize a report and may be used as index entries for cataloging the report. Key words must be selected so that no security classification is required. Identifiers, such as equipment model designation, trade name, military project code name, geographic location, may be used as key words but will be followed by an indication of technical context. The assignment of links, roles, and weights is optional.